

PREPARED FOR SUBMISSION TO JHEP

CERN-TH-2018-082
LAPTH-014/18
OUTP-17-18P

NNLOPS accurate associated HZ production with NLO decay $H \rightarrow b\bar{b}$

William Astill,^a Wojciech Bizoń,^a Emanuele Re,^{b,c} Giulia Zanderighi^{1c}

^a*Rudolf Peierls Centre for Theoretical Physics, Clarendon Laboratory, Parks Road, Oxford, UK*

^b*LAPTh, CNRS, Université Savoie Mont Blanc, 74940 Annecy, France*

^c*Theoretical Physics Department, CERN, Geneva, Switzerland*

E-mail: william.astill@physics.ox.ac.uk,

wojciech.bizon@physics.ox.ac.uk, emanuele.re@lapth.cnrs.fr,

giulia.zanderighi@cern.ch

ABSTRACT: We present a next-to-next-to-leading order (NNLO) accurate description of associated HZ production, followed by the Higgs boson decay into a pair of b -quarks treated at next-to-leading order (NLO), consistently matched to a parton shower (PS). The matching is achieved by performing reweighting of the HZJ-MiNLO events, using multi-dimensional distributions that are fully-differential in the HZ Born kinematics, to the NNLO results obtained by using the MCFM-8.0 fixed-order calculation. Additionally we include the $gg \rightarrow HZ$ contribution to the discussed process that appears at the $\mathcal{O}(\alpha_s^2)$. We present phenomenological results obtained for 13 TeV hadronic collisions.

KEYWORDS: QCD, Phenomenological Models, Hadronic Colliders, Monte Carlo, LHC

¹Rudolf Peierls Centre for Theoretical Physics, Clarendon Laboratory, Parks Road, Oxford, UK

Contents

1	Introduction	1
2	Outline of the method	3
2.1	HZJ-MiNLO with $H \rightarrow b\bar{b}$ decay at NLO	4
2.2	Phase-space parametrisation	5
2.3	Reweighting procedure	6
2.4	Treatment of the $gg \rightarrow HZ$ contribution	7
3	Practical implementation	8
3.1	Codes and settings	8
3.2	Interface to Parton Shower	9
4	Validation	10
5	Phenomenological results	13
6	Conclusions	20
A	Treatment of the $H \rightarrow b\bar{b}$ decay at NLO	22
B	Spectral decomposition of polar angle distributions	23
C	Hadronic tensor approach to matrix element	24
D	Impact of the $gg \rightarrow HZ$ contributions	26

1 Introduction

After the discovery of the Higgs boson in Run I [1, 2], one of the main tasks of the ongoing LHC Run II is to perform accurate measurements of Higgs properties. In order to carry out this precision physics program, it is important to study Higgs production in all the main production modes, and compare measurements with theory predictions, for total cross sections and differential distributions. An important goal which is expected to be achievable with the Run II full luminosity is to establish solid statistical evidence for HV associated production [3, 4].

The past years have seen a remarkable progress in NNLO QCD calculations, and, currently, all $2 \rightarrow 2$ SM scattering processes are known to this accuracy, see *e.g.* ref. [5]. Thanks to this progress, the description of colour singlet final states has reached a high level of accuracy. This is particularly true for processes where, at leading order (LO), there are no gluons in the initial state: in this case higher-order corrections are typically

moderate, and hence including NNLO corrections leads to very stable results, with small perturbative uncertainties. For HZ production, the NNLO corrections have been computed for the inclusive cross section [6] as well as for differential distributions [7–9]. Electroweak corrections for this process are also known at NLO for inclusive cross sections and differential distributions [10, 11], and are implemented in the public code **HAWK** [12]. Notably, NLO electroweak and QCD corrections were simultaneously matched to a parton shower in ref. [13] for HV and HV+jet, using, in the latter case, the **MinLO** method (to be described below).

Since associated HV production has a small cross section, it is often considered in association with a Higgs boson decaying to a b -quark pair, which is the largest Higgs decay mode. In this case properties of the b -jets arising from the Higgs decay products are used in experimental analysis to enhance the signal over SM backgrounds, and they will also be important for extracting precise information on the b -quark Yukawa coupling, especially in the Higgs boosted regime. Because of this, including QCD corrections to the $H \rightarrow b\bar{b}$ decay is particularly important, especially since these corrections are known to be large. The QCD NLO corrections to the Higgs decay to massive b -quarks have been known for a long time [14–17], whereas more recently NNLO corrections were computed in refs. [18, 19] for massless b -quarks. In the last few years the focus has moved towards a combination of the aforementioned fully-differential NNLO computations for $pp \rightarrow HV$ with differential NLO and NNLO results for $H \rightarrow b\bar{b}$. The current state-of-the-art results are those obtained in refs. [9, 20], where the fully-differential QCD NNLO computations for $pp \rightarrow HV$ and $H \rightarrow b\bar{b}$ (in the limit of massless b -quarks) have been combined together.

The precision of theory predictions is usually quantified in terms of renormalisation and factorisation scale variation of the NNLO results. It is however also known that all-order effects can be sizeable and can give rise to effects that are outside the fixed-order scale uncertainty band. For this reason, a lot of effort is put into combining NNLO calculations with parton shower effects, thereby obtaining so-called NNLOPS generators. Three methods have been suggested recently to achieve this accuracy. The **UNNLOPS** approach, which has been used for Drell-Yan [21] and Higgs production [22], is based on partitioning the phase space into an unresolved and a one-jet region and a subsequent matching to parton shower for the resolved one-jet region. The **Geneva** approach [23] instead uses the next-to-next-to-leading logarithmic (NNLL) accurate resummation for a specific observable to essentially partition the phase space. This method has been applied recently to Drell-Yan production [23]. Finally, the **MinLO** approach [24, 25] relies on first using **MinLO** to achieve an NLO merging of the processes with the production of the colour-singlet state (X) and the same processes with one additional jet ($X + 1$ jet), and on performing a reweighing of the **MinLO** $X + 1$ jet events to NNLO Born distributions for X . This method has been applied recently to Higgs production [26, 27], Drell-Yan [28] and HW production [29].

In this paper we consider the production of a Higgs boson in association with a Z boson and consider the decay of the Higgs to bottom quarks, the decay mode with the largest branching ratio, and the decay of the Z boson to leptons. We build a Monte Carlo that is NNLO accurate in production, preserves NLO accuracy in the decay and includes parton shower effects. We also include the NNLO $gg \rightarrow HZ$ channel at leading order in

production, including LO corrections in decay and parton shower effects. This subprocesses is added separately, and we assess its numerical impact. Our implementation uses and adapts the `POWHEG-BOX-RES` code, which is based on `POWHEG-BOX-V2` but has a resonant-aware treatment of internal resonances [30], and hence it is suited to treat NLO corrections to production and decay.

The paper is organised as follows. In Sec. 2 we outline the method used to obtain NNLOPS accurate predictions including the NLO treatment of the decay. In particular we explain how the latter is included together with MiNLO within the `POWHEG-BOX-RES` framework. We detail how we parametrise the phase-space, and also explain how we treat the $\mathcal{O}(\alpha_s^2)$ $gg \rightarrow HZ$ contribution. In Sec. 3 we give details about our practical implementation, as well as about our interface to the parton shower. In Sec. 4 we validate our results by checking that we reproduce NNLO results for Born-like observables, also for variables not used for the reweighting. In Sec. 5 we present distributions with fiducial cuts inspired by the recent ATLAS analysis of ref. [3]. Finally, we present our conclusions in Sec. 6. A number of Appendices provide more details about the treatment of the decay at NLO, the spectral decomposition that we use to parametrise the phase space, the dependence of the matrix element on the extra polar angle used in the phase-space parametrisation, and the impact of $gg \rightarrow HZ$ contribution.

2 Outline of the method

In this work we consider the production of a Higgs boson in association with a Z boson, followed by the Z boson decay into a pair of leptons and the Higgs boson decay into pair of b -quarks

$$pp \longrightarrow HZ \longrightarrow (b\bar{b}) (\ell^+ \ell^-). \quad (2.1)$$

The decay of the Z boson is treated exactly with all spin correlations between initial and final-state fermions taken into account. The decay of the Higgs boson is treated in the narrow-width approximation at next-to-leading order in QCD.

In order to achieve NNLOPS accuracy we follow the method of reweighting Les Houches events (LHE), produced by MiNLO improved HZJ generator (HZJ-MiNLO), with NNLO accurate fixed-order predictions, differential in the Born phase space. The procedure was first proposed in [25] and later implemented for various colour-singlet production processes [26–29]. In its simplest implementation, the method consists in reweighting LHE event samples obtained with the HZJ-MiNLO generator using multi-differential HZNNLO distributions, with the factor

$$\mathcal{W}(\Phi_{\ell\bar{\ell}b\bar{b}}) = \frac{d\sigma_{\text{NNLO}}(\Phi_{\ell\bar{\ell}b\bar{b}})}{d\sigma_{\text{MiNLO}}(\Phi_{\ell\bar{\ell}b\bar{b}})}, \quad (2.2)$$

where $\Phi_{\ell\bar{\ell}b\bar{b}}$ is the Born phase-space of process (2.1). The resulting event sample (which we refer to by HZ-MNLOPS(LHEF)) is NNLO accurate: by construction the method provides NNLO accuracy for all Born distributions and 1-jet observables remain NLO accurate since the reweighting factor differs from one by $\mathcal{O}(\alpha_s^2)$ corrections. For the proof we refer the reader to [26, 28]. Furthermore, a subsequent parton shower will not spoil the claimed accuracy provided that the hardest real radiation for each event is generated by `POWHEG`

itself. This procedure was applied recently to HW production in ref. [29], hence we refer the reader to that paper for further details. Instead, in this section, we first give a detailed description of the treatment of the NLO $H \rightarrow b\bar{b}$ decay, which is the new element of this work (Sec. 2.1). We then give some technical details on how the reweighting to NNLO was achieved (Sec. 2.2 and 2.3), and, finally, in Sec. 2.4 we discuss the inclusion of the loop-induced $gg \rightarrow HZ$ process, which is part of the NNLO corrections to $pp \rightarrow HZ$.

2.1 HZJ-MiNLO with $H \rightarrow b\bar{b}$ decay at NLO

In this work we use the MiNLO prescription only for the production part of the process, and match this to a “resonance improved” POWHEG implementation of the NLO QCD calculation of the $H \rightarrow b\bar{b}$ decay. As described in the previous subsection, we treat the Higgs boson decay in the narrow-width approximation (NWA).

We start by introducing the \bar{B} function [31] that we use in our HZJ code, which reads schematically

$$\begin{aligned} \bar{B} = & \alpha_s(q_t^2) \Delta_q^2(Q, q_t) \frac{\text{Br}(H \rightarrow b\bar{b})}{\Gamma_{\text{NLO}}} \left[B_{\text{HZJ}} (1 - 2\Delta_q^{(1)}(Q, q_t)) d\Gamma_{b\bar{b}}^{(0)} \right. \\ & \left. + \left(V_{\text{HZJ}} + \int d\phi_r R_{\text{HZJ}}(\phi_r) \right) d\Gamma_{b\bar{b}}^{(0)} + B_{\text{HZJ}} \left(d\Gamma_{b\bar{b}}^{(V)} + \int d\phi_r d\Gamma_{b\bar{b}}^{(R)}(\phi_r) \right) \right], \end{aligned} \quad (2.3)$$

where the Higgs propagator is left implicit; $\text{Br}(H \rightarrow b\bar{b})$ is the best prediction for the Standard Model $H \rightarrow b\bar{b}$ branching ratio; and $d\Gamma_{b\bar{b}}^{(0/V/R)}$ are the Born, virtual, and real squared amplitudes for the $H \rightarrow b\bar{b}$ decay, differential in their kinematics. $\Gamma_{\text{NLO}} = \Gamma_{b\bar{b}}^{(0)} + \Gamma_{b\bar{b}}^{(1)}$ denotes the NLO accurate $H \rightarrow b\bar{b}$ partial decay width. With $\Delta_q(Q, q_t)$ we denote the MiNLO Sudakov form factor for quark induced boson production (see ref. [25] for its precise definition) and $\Delta_q^{(1)}(Q, q_t)$ is its $\mathcal{O}(\alpha_s)$ expansion. The hard scale in the Sudakov is set to $Q^2 = (p_Z + p_H)^2$ and q_t is the transverse momentum of the HZ system, where the Higgs is obtained from the sum of the momenta of its decay products ($b\bar{b}$ or $b\bar{b}g$). In the formula above the additional α_s factor in the NLO correction is contained implicitly in the V and R functions, as well as in $d\Gamma_{b\bar{b}}^{(V)}$ and $d\Gamma_{b\bar{b}}^{(R)}$. In the former two, following the MiNLO prescription, we set the central renormalisation scale to $\mu_R = q_t$, whereas for the decay we set the central scale to $\mu_R = M_H$ since this is the natural scale for the decay and no MiNLO procedure is applied to it (in App. A we denote as μ_r the renormalisation scale for the decay).

If we integrate Eq. (2.3) over the phase space of all final-state light partons we obtain

$$d\sigma_{\text{MiNLO}}(\Phi_{\ell\bar{\ell}b\bar{b}}) = \text{Br}(H \rightarrow b\bar{b}) \cdot \left[\left(d\sigma_{\text{HZ}}^{(0)} + d\sigma_{\text{HZ}}^{(1)} \right) \cdot \frac{d\Gamma_{b\bar{b}}^{(0)} + d\Gamma_{b\bar{b}}^{(1)}}{\Gamma_{\text{NLO}}} + d\tilde{\sigma}_{\text{HZ}}^{(2)} \cdot \frac{d\Gamma_{b\bar{b}}^{(0)}}{\Gamma_{\text{NLO}}} \right] + \mathcal{O}(\alpha_s^3), \quad (2.4)$$

where

$$d\Gamma_{b\bar{b}}^{(1)} = d\Gamma_{b\bar{b}}^{(V)} + \int d\phi_r d\Gamma_{b\bar{b}}^{(R)}(\phi_r), \quad (2.5)$$

and $d\sigma_{\text{HZ}}^{(i)}$ denotes the $\mathcal{O}(\alpha_s^i)$ correction to the HZ production cross section. The $d\tilde{\sigma}^{(2)}$ denotes the $\mathcal{O}(\alpha_s^2)$ part of the HZJ-MiNLO computation, which corresponds to double-real and real-virtual parts of HZ production at NNLO.

We obtain NNLO prediction (*without* the loop-induced $gg \rightarrow \text{HZ}$ contribution, which is discussed in Sec. 2.4) for the production combined with NLO corrections to the decay from MCFM-8.0, whose output is

$$d\sigma_{\text{NNLO}}(\Phi_{\ell\bar{\ell}b\bar{b}}) = \text{Br}(\text{H} \rightarrow b\bar{b}) \cdot \left[d\sigma_{\text{HZ}}^{(0)} \cdot \frac{d\Gamma_{b\bar{b}}^{(0)} + d\Gamma_{b\bar{b}}^{(1)}}{\Gamma_{\text{NLO}}} + (d\sigma_{\text{HZ}}^{(1)} + d\sigma_{\text{HZ}}^{(2)}) \cdot \frac{d\Gamma_{b\bar{b}}^{(0)}}{\Gamma_{b\bar{b}}^{(0)}} \right]. \quad (2.6)$$

It is easy to check that after integrating out the decay of the Higgs boson in equation (2.6) one recovers the fully inclusive NNLO result multiplied by the overall branching ratio. One can also easily verify that

$$\mathcal{W}(\Phi_{\ell\bar{\ell}b\bar{b}}) = \frac{d\sigma_{\text{NNLO}}(\Phi_{\ell\bar{\ell}b\bar{b}})}{d\sigma_{\text{MiNLO}}(\Phi_{\ell\bar{\ell}b\bar{b}})} = 1 + \frac{(\sigma^{(2)} - \tilde{\sigma}^{(2)})}{\sigma^{(0)}} + \mathcal{O}(\alpha_s^3), \quad (2.7)$$

which means that reweighting HZJ-MiNLO events with this factor does not spoil the NLO accuracy of the event sample in the HZ+jet region, since the rescaling is equal to one up to $\mathcal{O}(\alpha_s^2)$ terms. In the following section we describe how we proceed to obtain distributions differential in the Born phase space $\Phi_{\ell\bar{\ell}b\bar{b}}$.

2.2 Phase-space parametrisation

Our Born phase space contains four final-state particles, two leptons (ℓ^+, ℓ^-) and two bottom quarks (b, \bar{b}). After neglecting an irrelevant azimuthal angle and upon inclusion of the initial-state degrees of freedom we are left with 9 independent dimensions. Furthermore we can factorise the Born phase-space as follows:

$$d\Phi_{\ell\bar{\ell}b\bar{b}} = d\Phi_{\text{H}\ell\bar{\ell}} \times (2\pi)^3 dq^2 \times d\Phi_{\text{H} \rightarrow b\bar{b}}, \quad (2.8)$$

where q^2 is the virtuality of the Higgs boson, $\Phi_{\text{H}\ell\bar{\ell}}$ is the 6-dimensional phase space for the production of an undecayed Higgs boson with a pair of leptons from the decay of the associated Z boson, and $\Phi_{\text{H} \rightarrow b\bar{b}}$ is the 2-dimensional phase space for the decay of a Higgs boson into a pair of b -quarks. By working in the NWA we perform a reweighting only on the first part of the phase-space $\Phi_{\text{H}\ell\bar{\ell}}$, as the decay is already treated at the required accuracy (NLO) in our implementation of HZJ-MiNLO.

A parametrisation of $\Phi_{\text{H}\ell\bar{\ell}}$ can be defined in a number of ways. After careful considerations we have chosen the invariant mass and rapidity of the HZ system (M_{HZ} and y_{HZ}) to be the first two variables. As a third variable we choose $\cos\alpha$, where α is the polar angle of the Z boson with respect to the beam axis in the frame where the HZ system is at rest, *i.e.*

$$\cos\alpha = \frac{\vec{p}'_Z \cdot \hat{z}'}{|\vec{p}'_Z| |\hat{z}'|}, \quad (2.9)$$

where $'$ indicates that directions are expressed in the HZ rest-frame and the original \hat{z} direction is along the beam axis. Subsequently we choose the invariant mass of the Z boson, $M_{\ell\bar{\ell}}$, and a convenient choice for the last two dimensions is to use Collins-Soper angles (θ^*, ϕ^*) defined in [32]. In summary the full phase space parametrisation reads

$$\Phi_{\text{H}\ell\bar{\ell}} = \{M_{\text{HZ}}, y_{\text{HZ}}, \cos\alpha, M_{\ell\bar{\ell}}, \theta^*, \phi^*\}. \quad (2.10)$$

Following the arguments of [32] and the discussion in Sec. 2 of [29] we parametrise the (θ^*, ϕ^*) -dependence as follows:

$$\begin{aligned} \frac{d\sigma}{d\Phi_{H\ell\bar{\ell}}} &= \frac{d^6\sigma}{dM_{\text{HZ}} dy_{\text{HZ}} d\cos\alpha d\cos\theta^* d\phi^*} \\ &= \frac{3}{16\pi} \left(\frac{d\sigma}{d\Phi_{\text{HZ}}} (1 + \cos^2\theta^*) + \sum_{i=0}^7 A_i(\Phi_{\text{HZ}}) f_i(\theta^*, \phi^*) \right), \end{aligned} \quad (2.11)$$

where in the second line we have used a short notation for the phase-space without leptonic angles

$$\Phi_{\text{HZ}} = \{M_{\text{HZ}}, y_{\text{HZ}}, \cos\alpha\}. \quad (2.12)$$

The complete set of functions $f_i(\theta^*, \phi^*)$, together with a procedure for extracting coefficients $A_i(\Phi_{\text{HZ}})$, is given in equations (2.3-2.4) of ref. [29]. We note that for practical purposes we will use only the first five A_i coefficients (A_0, \dots, A_4) and, for simplicity, we neglect the remaining three (A_5, A_6, A_7) since their impact on any distribution that we examined is numerically negligible.

Finally, we can parametrise the dependence on the Z boson polar angle α (see Eq. (2.9)) using a set of orthonormal functions $g_j(\cos\alpha)$. The definition of the basis elements g_j is given in App. B. With this choice we have

$$\begin{aligned} \frac{d\sigma}{d\Phi_{\text{HZ}}} &= \sum_{j=0}^N c_j(\Phi) g_j(\cos\alpha), \\ A_i(\Phi_{\text{HZ}}) &= \sum_{j=0}^N a_{ij}(\Phi) g_j(\cos\alpha), \end{aligned} \quad (2.13)$$

where c_j and a_{ij} are coefficients depending on $\Phi = \{M_{\text{HZ}}, y_{\text{HZ}}\}$ and N is the upper limit of the sum, which in general can be inferred by analysing the matrix elements contributing to the cross section. We investigate the matrix elements in App. C and find that, at most, polynomials of 5th-degree in the $\cos\alpha$ and $\sin\alpha$ variables can appear. Accordingly, we set $N = 10$ in Eq. (2.13).

To summarise, our parametrisation of the fully differential cross section as used in the reweighting procedure reads

$$\frac{d\sigma}{d\Phi_{H\ell\bar{\ell}}} = \frac{3}{16\pi} \sum_{j=0}^{10} \left(c_j(\Phi) (1 + \cos^2\theta^*) + \sum_{i=0}^7 a_{ij}(\Phi) f_i(\theta^*, \phi^*) \right) g_j(\cos\alpha), \quad (2.14)$$

where the functions $g_j(\cos\alpha)$ are defined in Eq. (B.5) and the coefficients $c_j(\Phi)$ and $a_{ij}(\Phi)$ can be obtained from Eq. (2.13) by exploiting the orthonormality of the g_j functions.

2.3 Reweighting procedure

The reweighting procedure leaves some degree of freedom for the user. The simple rescaling with a factor, presented in (2.2), spreads the corrections uniformly over the whole phase-space. However we know that regions where the HZ system is accompanied by hard QCD

radiation is equally well described by both predictions, HZNNLO and HZJ-MiNLO. Hence, it is desirable to limit the corrections to the phase space with no hard jet. To achieve this, we proceed along the lines of the prescription presented in [26]. We split the cross section into two parts

$$d\sigma_A = d\sigma h(p_t), \quad d\sigma_B = d\sigma (1 - h(p_t)), \quad (2.15)$$

where

$$h(p_t) = \frac{(M_H + M_Z)^2}{(M_H + M_Z)^2 + p_t^2}, \quad (2.16)$$

and p_t is the transverse momentum of the leading jet, computed here using the k_t -algorithm with $R = 0.4$. With such a choice Eq. (2.2) takes form

$$\begin{aligned} \mathcal{W}(\Phi_{H\ell\bar{\ell}}, p_t) = h(p_t) & \frac{\int d\sigma_{\text{NNLO}} \delta(\Phi_{H\ell\bar{\ell}} - \Phi_{H\ell\bar{\ell}}(\Phi)) - \int d\sigma_{\text{MiNLO},B} \delta(\Phi_{H\ell\bar{\ell}} - \Phi_{H\ell\bar{\ell}}(\Phi))}{\int d\sigma_{\text{MiNLO},A} \delta(\Phi_{H\ell\bar{\ell}} - \Phi_{H\ell\bar{\ell}}(\Phi))} \\ & + (1 - h(p_t)). \end{aligned} \quad (2.17)$$

This procedure smoothly turns off the corrections when moving to regions of phase space with hard emissions whilst preserving the total cross section,

$$\left(\frac{d\sigma}{d\Phi_{H\ell\bar{\ell}}} \right)_{\text{NNLOPS}} = \left(\frac{d\sigma}{d\Phi_{H\ell\bar{\ell}}} \right)_{\text{NNLO}}. \quad (2.18)$$

It is worth noting that choosing the transverse momentum p_t in Eq. (2.16) as the transverse momentum of hardest jet is not equivalent to choosing the transverse momentum of the colour-singlet, the difference being due to configurations where the colour-singlet has small transverse momentum and it is accompanied by hard QCD emissions whose transverse momenta counterbalance each other. The latter configurations dominate in the region where $p_{t,\text{HZ}} \sim 0$.

In the next section we will explain how we have included in our simulation the loop-mediated $gg \rightarrow \text{HZ}$ contribution, which was not included in $d\sigma_{\text{NNLO}}$ (and hence not even in the reweighting factor defined in Eq. (2.17)), whilst being formally $\mathcal{O}(\alpha_s^2)$.

2.4 Treatment of the $gg \rightarrow \text{HZ}$ contribution

The $\mathcal{O}(\alpha_s^2)$ contributions of the form $gg \rightarrow \text{HZ}$, that appear in the process of Higgs boson production in association with a Z boson, originate from the squared 1-loop diagrams shown for example in Fig. 5 of ref. [8]. There are two classes of contributions: box diagrams involving a Yukawa coupling of the Higgs boson, and triangle diagrams where the Higgs boson is radiated from the Z boson which couples to the fermion loop. Both contributions vanish trivially when massless quarks of the first and second generation run in the loop. These $gg \rightarrow \text{HZ}$ contributions are known to constitute a significant part of the cross section [7, 8, 20, 33, 34], especially when the invariant mass of the produced HZ system is larger than twice the top-quark mass. Being loop-induced, so far only approximate NLO corrections are known for this channel [35, 36]. On the other hand, their loop origin makes these terms particularly sensitive to New Physics [37–39].

In our reweighting procedure we do not include this contribution, but we will treat it independently using a separate event sample produced using a leading order implementation

of loop-induced $gg \rightarrow HZ$ process implemented in POWHEG [40], which includes top and bottom quarks in the loop.¹ We note that the $gg \rightarrow HZ$ contribution can be treated separately since it is finite. Furthermore, parton shower radiation from gluon-initiated hard processes is typically different from processes also involving initial-state quarks. From that point of view, it is important not to include the $gg \rightarrow HZ$ contribution through a simple reweighting. Further discussion of the $gg \rightarrow HZ$ channel is presented in App. D. For this contribution we do not include any radiative correction to the $H \rightarrow b\bar{b}$ decay, hence the radiation from the decay is fully taken care of by Pythia8. Higher-order NLO corrections to this decay could also be included with relatively little effort.

3 Practical implementation

In this section we first discuss the codes used to obtain our predictions, as well as the relevant settings and the parameters. We also describe subtleties related to the interface to Pythia8 when radiation from resonances is taken into account.

3.1 Codes and settings

In order to obtain an ensemble of NNLOPS accurate Les Houches events for the process in Eq. (2.1) we need fully differential predictions from an NNLO fixed-order calculation, and an NLO accurate event-sample for HZJ production improved with the MiNLO prescription.

For the NNLO fixed-order prediction we use the MCFM-8.0 calculation [8]. In order to obtain both the NNLO accuracy for the production of the HZ resonance as well as the NLO accuracy of hadronic decay of Higgs boson, $H \rightarrow b\bar{b}$, we perform two separate runs of the program with `nproc=101` at the `'nnlo'` order (for the first) and `nproc=1010` at the `'nlo'` order (for the latter). The prediction presented in Eq. (2.6) is simply obtained by adding results of the two runs. As it was pointed out in Sec. 2.1 and Sec. 2.4, we do not include $gg \rightarrow HZ$ contributions in the reweighting procedure. To remove them we have modified part of the MCFM-8.0 code, which computes double-virtual corrections. We will include this contribution in our phenomenological analysis in Sec. 5, as stated clearly in the appropriate places.

The initial sample of Les Houches events is generated using the HZJ-MiNLO package, originally in POWHEG-BOX-V2, which we adapted to run in POWHEG-BOX-RES [30]. We have also extended the original package to include NLO corrections of the Higgs boson decay into pair of b -quarks, as discussed in Sec. 2.1. The relevant matrix elements have been reported in App. A. Despite the fact that there is no interference between production and decay, in order to treat the radiation from the resonance we have made use of the POWHEG-BOX-RES framework [30].

In our work we use PDF4LHC15_nnlo_mc parton distribution functions [41–44]. We set $M_H = 125.0$ GeV, $\Gamma_H = 4.088$ MeV, $M_Z = 91.1876$ GeV, and $\Gamma_Z = 2.4952$ GeV. Moreover $G_F = 1.16639 \cdot 10^{-5} \text{GeV}^{-2}$, $\sin^2 \theta_W = 0.2223$, $\alpha_{\text{EM}}(M_Z) = 128.89$, and $\text{Br}(H \rightarrow b\bar{b}) = 0.5824$.

For the contributions where the Higgs boson is radiated from a heavy-quark loop we use pole mass of the heavy quark as it is usually done in publicly available codes [8]. In

¹The code can be obtained from `svn://powhegbox.mib.infn.it/trunk/User-Processes-V2/ggHZ`.

particular we set pole mass of the bottom quark to $m_b = 4.92$ GeV and pole mass of the top quark to $m_t = 173.2$ GeV. Moreover, for the bottom Yukawa coupling in $H \rightarrow b\bar{b}$ decay we use its $\overline{\text{MS}}$ running mass evaluated at scale M_H . The running masses are computed from the pole masses using an $\mathcal{O}(\alpha_s^2)$ conversion [45] and the numerical value of the $\overline{\text{MS}}$ mass for the bottom quark, obtained by running the strong coupling using LHAPDF, is $m_b(M_H) = 3.16$ GeV.

The NNLO fixed-order prediction is obtained using fixed renormalisation and factorisation scale equal to sum of the Higgs boson and the Z boson mass, $\mu = M_H + M_Z$. The scale choice in HZJ-MiNLO case for the production is fixed by MiNLO procedure [24], while for the decay the central scale choice is M_H , as explained in Sec. 2.1. We estimate the theoretical uncertainty using 7 point scale variation for both fixed-order NNLO results as well as MiNLO predictions. The scale variation in production and decay are always correlated (this includes the decay renormalisation scale, *i.e.* the scale at which we evaluate the $\overline{\text{MS}}$ b -quark mass). We perform correlated variations in MCFM-8.0 and HZJ-MiNLO, that is, our final uncertainty is an envelop of 7 scale combinations, *i.e.* for a given (K_r, K_f) choice in HZJ-MiNLO we use the same choice in MCFM-8.0 and as usual we consider variations of the central scale by a factor two up and down, restricted to $1/2 \leq K_r/K_f < 2$. The $gg \rightarrow \text{HZ}$ contribution is then added with the same (K_r, K_f) choice.

When interfacing our fixed-order predictions to a parton shower we use Pythia8 [46], as detailed more precisely in the next subsection. Unless stated otherwise, predictions are shown at parton level, with no multi-parton interactions.

3.2 Interface to Parton Shower

In order to combine our results with a parton shower we follow an approach similar to the one first introduced for the NLO $t\bar{t}$ production treatment in [47], that allows for a generation of radiation also from resonances. In our simulation we set the flag `allrad` to 0, which means that the NLO POWHEG emission is generated at most from one singular region, associated either with the production stage or with the radiation from a resonance and we do not consider radiation from multiple regions. This is the standard POWHEG procedure to generate the hardest radiation. In this configuration POWHEG uses the usual highest bid mechanism to choose the origin of the emission.

For the parton shower we use Pythia8. A requirement for the matching to the parton shower to work properly is that the hardest radiation should be the one generated by POWHEG. This is usually achieved by setting a value of `scalup` in every event, which sets the veto scale for the parton shower. One subtlety is however that the definition of the hardness of the radiation from the decay in POWHEG and Pythia8 differ. As a consequence, after an event is showered, we recompute the hardness of the first emission generated by Pythia8 using the POWHEG formula and accept the showered event only if this hardness is lower than the `scalup` value of the given event. If this is not the case, we shower the event again until the new showered event meets the required condition. Details of the hardness definition used in POWHEG and Pythia8 are given in App. A of ref. [47]. We have checked that our procedure to veto radiation gives results that are fully compatible with those obtained by the procedure encoded in the `PowhegHooks`-class provided by Pythia8 [46].

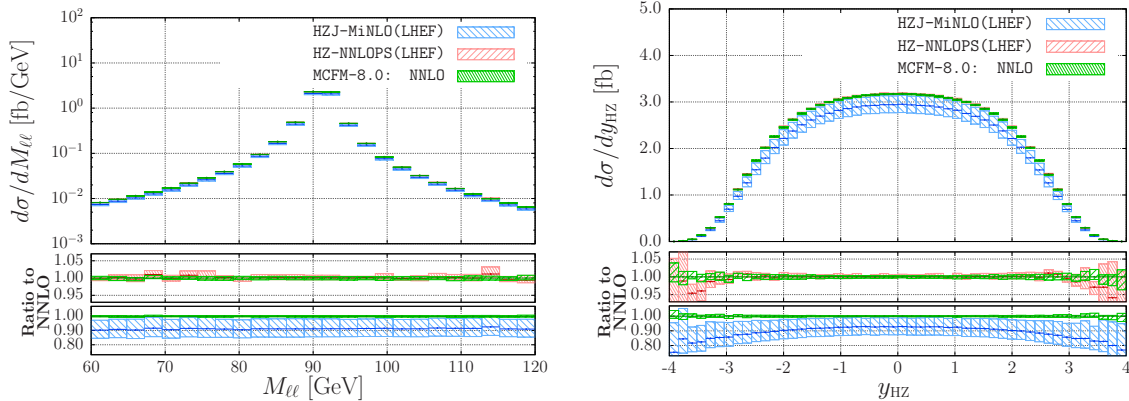


Figure 1. The differential distributions of the invariant mass of final-state leptons $M_{\ell\bar{\ell}}$ (left panel) and the distribution of the rapidity of the HZ system y_{HZ} (right panel). The one-loop squared terms from the $gg \rightarrow \text{HZ}$ channel have not been included.

4 Validation

In the following section we present the validation of our results. We carefully compare distributions prepared from reweighted Les Houches events (HZ-NNLOPS(LHEF)) with the ones obtained using fixed-order NNLO code (MCFM-8.0). We remind the reader that, in the reweighting procedure, we don't take into account one-loop squared contributions arising from $gg \rightarrow \text{HZ}$ channel, as specified and motivated in Sec. 2.3 and 2.4 respectively. Therefore all the plots of this section do not contain the $gg \rightarrow \text{HZ}$ channel, which instead will be included in Sec. 5.

In the plots of this section, the blue, green and red markers represent results from HZJ-MiNLO Les Houches events, the fixed-order calculation obtained with MCFM-8.0, and the reweighted HZ-NNLOPS(LHEF) event sample, respectively. The uncertainty band represents the usual scale variation uncertainty, as described in detail in the previous section.

The first pair of plots that we want to present is the distribution of the invariant mass of final-state leptons $M_{\ell\bar{\ell}}$ and the distribution of the rapidity of the HZ system y_{HZ} , which are shown in the left and right panel of Fig. 1, respectively. We start by noting that the ratio of MCFM-8.0 to HZJ-MiNLO, bottom panel of Fig. 1, is constant, which is along the lines of our assumption that the reweighting factor $\mathcal{W}(\Phi_{\ell\bar{\ell}b\bar{b}})$ should be constant along the $M_{\ell\bar{\ell}}$ direction. We do not repeat the thorough procedure of validation, which was included in our previous work [29]. The distribution of y_{HZ} , right panel of Fig. 1, is again properly reproduced by our calculation across the whole spectrum. We take note of the fact that the discrepancies at the edges of the distribution are in the regions of phase-space which are poorly populated. More precisely, having used distributions with varying bin-size for the reweighting, all events with $y_{\text{HZ}} \lesssim -3$ (or $y_{\text{HZ}} \gtrsim +3$) fall into the first (or the last) bin of the differential reweighting factor $\mathcal{W}(\Phi_{\ell\bar{\ell}b\bar{b}})$. The description of the forward rapidity region can be improved by increasing the statistics of the multi-differential distributions and by including more bins at large rapidity. In Fig. 2, we present the differential distribution of M_{HZ} in two different mass regions. For this distribution the difference between HZJ-MiNLO

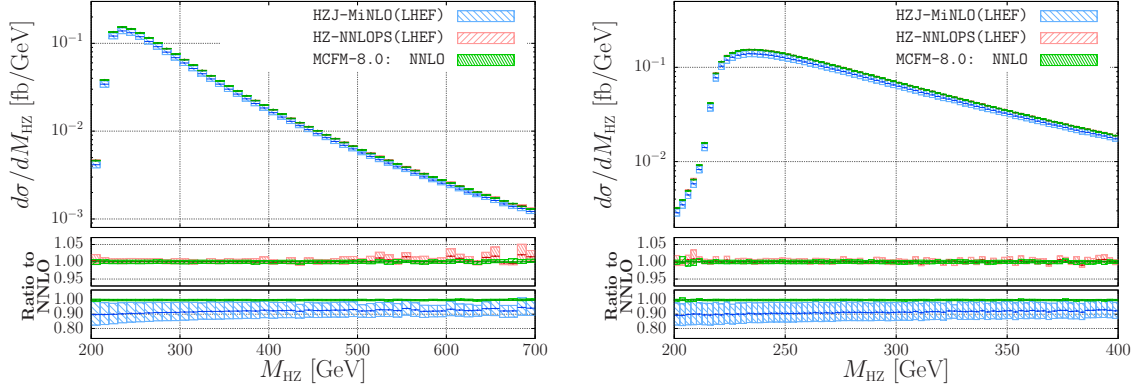


Figure 2. The differential distributions of the invariant mass of the HZ system M_{HZ} in two different mass regions. The one-loop squared terms from $gg \rightarrow \text{HZ}$ channel have not been included.

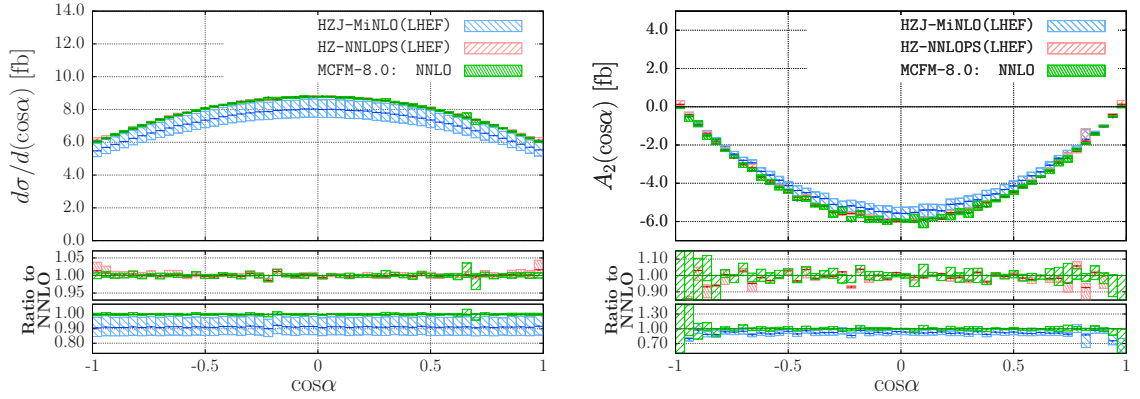


Figure 3. The differential distributions of the Z boson polar angle with respect to the beam axis, defined in Eq. (2.9): differential cross section as a function of $\cos\alpha$ (left panel) and the dependence of coefficient $A_2(\cos\alpha)$, see Eq. (2.11). The one-loop squared terms from the $gg \rightarrow \text{HZ}$ channel have not been included.

and the NNLO is small and flat over the whole range. After reweighting, we find perfect agreement between NNLO and HZ-NNLOPS(LHEF) results.

As the next step, we look closely at the differential distributions of the angular variables: $\cos\alpha$ and Collins-Soper angles. The distribution of $\cos\alpha$ is presented in Fig. 3. We recollect that this dependence was not just recorded as a histogram, but rather parametrised in terms of spectral modes, Eq. (2.13). This has improved the stability of the distribution, and as a consequence of the reweighting factor, which is very useful when working with samples of limited statistics. Further we check the quality of the reconstruction of the Collins-Soper angles. We present the relevant distributions in Fig. 4. In summary, we find that for all variables used for the reweighting, the NNLO and HZ-NNLOPS(LHEF) predictions agree within their statistical fluctuations.

To complete the validation, we also need to examine Born-like observables that were not used in the reweighting procedure. As such, we chose to look at transverse momentum and rapidity of the Higgs boson (see Fig. 5). We again confirm that both the central values

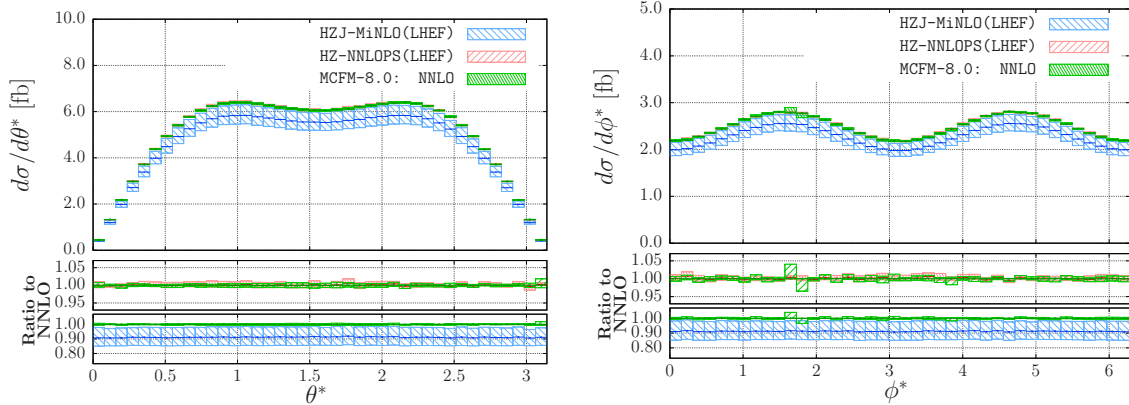


Figure 4. The differential distributions of Collins-Soper angles: θ^* (left) and ϕ^* (right). The one-loop squared terms from the $gg \rightarrow HZ$ channel have not been included.

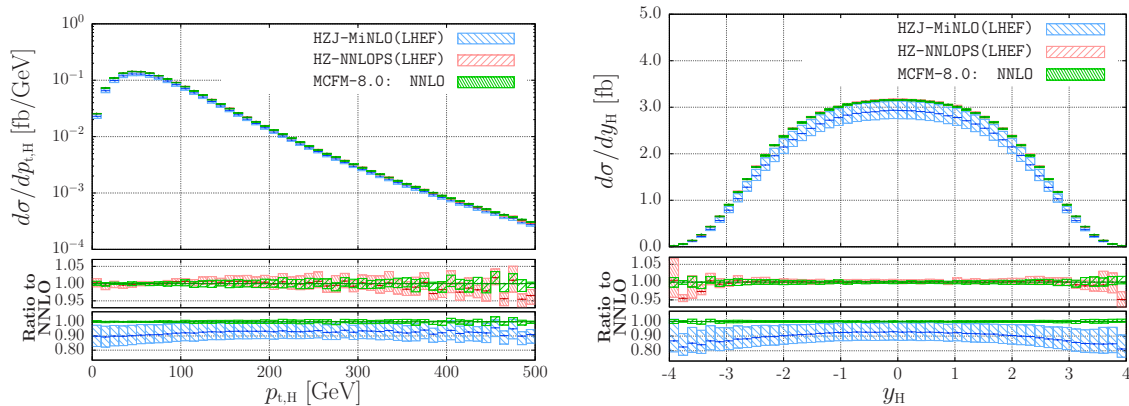


Figure 5. The differential distributions of the transverse momentum (left panel) and the rapidity (right panel) of the Higgs boson. The one-loop squared terms from the $gg \rightarrow HZ$ channel have not been included.

and scale variation bands are properly reconstructed within statistical fluctuations, which increase at high transverse momentum ($p_{t,H} \gtrsim 400$ GeV) and large rapidity ($|y_H| \gtrsim 3$). The agreement between NNLO and HZ-NNLOPS(LHEF) in these corners of phase space could be improved further by increasing the statistics of the reweighting factor and decreasing the bin-sizes in this region.

Finally we turn to the discussion of the distribution of the transverse momentum of HZ system, an observable which is singular at Born level but receives corrections due to QCD radiation at higher-orders in perturbation theory. We compare results obtained using two different reweighting prescriptions: the one described in Sec. 2.3, presented in the left plot of Fig. 6, and a setup where we set the function $h(p_t) \equiv 1$ in Eqs.(2.15)-(2.17), shown in the right hand side of Fig. 6. As expected, we observe that the HZJ-MiNLO and HZ-NNLOPS(LHEF) predictions feature a Sudakov damping at low transverse momentum, while the NNLO prediction diverges in this region. Furthermore, we observe that for the $h(p_t) = 1$ case, the HZ-NNLOPS(LHEF) results are uniformly shifted with respect to the orig-

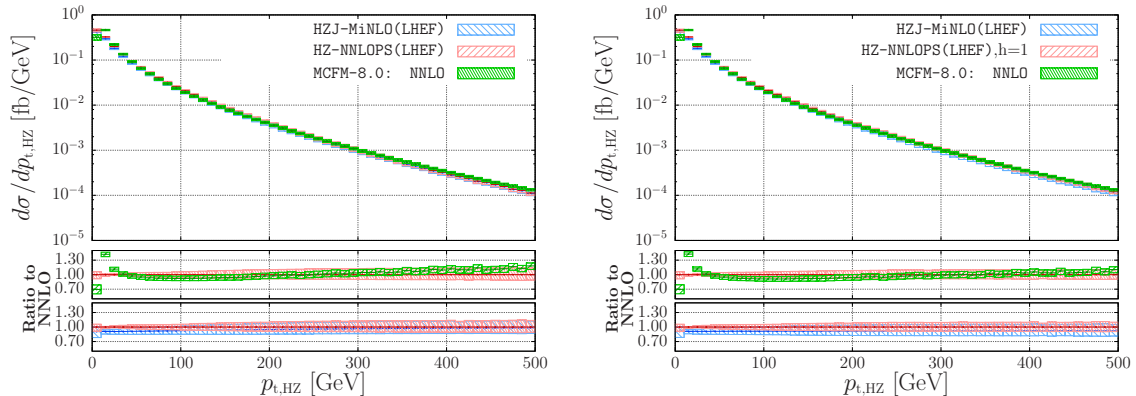


Figure 6. The differential distribution of the transverse momentum of the HZ system results when reweighting with damping factor $h(p_t)$ (left panel) or without (right panel). The one-loop squared terms from the $gg \rightarrow HZ$ channel have not been included.

inal event sample HZJ-MiNLO, as the reweighting factor $\mathcal{W}(\Phi_{H\ell\bar{\ell}})$ does not take into account any QCD radiation. Instead, when the reweighting factor depends on the transverse momentum of the leading jet, HZ-NNLOPS (LHEF) approaches the HZJ-MiNLO curve at high- $p_{t,HZ}$ values, as the effects of the reweighting are concentrated in the region of phase-space close to the Born kinematics, the natural habitat of $\mathcal{O}(\alpha_s^2)$ virtual corrections. In this case, the HZ-NNLOPS (LHEF) prediction at high transverse momentum agrees with the HZJ-MiNLO prediction, rather than with the pure NNLO result. We note that in this region, all predictions are only NLO accurate and that the former has a dynamical scale, dictated by the MiNLO prescription, while the NNLO uses a fixed renormalisation and factorisation scale choice, $M_H + M_Z$. Comparing the middle panels of Fig. 6, it might seem that the choice of a uniform reweighting provides a better description of the hard part of $p_{t,HZ}$ distribution, but the apparent agreement between MCFM-8.0 and HZ-NNLOPS (LHEF) results around 400-500 GeV is accidental. In fact, at even higher transverse momenta the NNLO result is above our HZ-NNLOPS (LHEF) prediction. This behaviour is entirely due to the aforementioned difference in scale choice.

5 Phenomenological results

In this section we turn to the discussion of the phenomenological results obtained with our new code. We stress again that we consider the production of a Higgs boson in association with a Z boson and their subsequent decays $H \rightarrow b\bar{b}$ and $Z \rightarrow \ell^+ \ell^-$, where in the following ℓ denotes a single leptonic species, *e.g.* e or μ . For the Higgs boson decay we include NLO QCD corrections.

We consider 13 TeV LHC collisions. We consider fiducial cuts inspired by the recent ATLAS analysis of ref. [3]. We require two charged leptons with $|y_\ell| < 2.5$ and $p_{t,\ell} > 7$ GeV, moreover the harder lepton should satisfy $p_{t,\ell} > 27$ GeV. We impose that the invariant mass of the leptons satisfies the condition $81 \text{ GeV} < M_{\ell\bar{\ell}} < 101 \text{ GeV}$. Additionally we require at least two b -jets with $|\eta_j| < 2.5$ and $p_{t,j} > 20$ GeV. Unless stated otherwise, jets are

Fiducial cross section	HZJ-MiNLO	MCFM-8.0	HZ-NNLOPS (LHEF)	HZNNLOPS
no $gg \rightarrow \text{HZ}$	$6.59^{+7.2\%}_{-6.2\%}$ fb	$7.14^{+0.5\%}_{-0.9\%}$ fb	$7.14^{+0.3\%}_{-0.4\%}$ fb	$6.49^{+0.8\%}_{-0.6\%}$ fb
with $gg \rightarrow \text{HZ}$	–	$7.92^{+2.0\%}_{-1.5\%}$ fb	$7.90^{+2.8\%}_{-2.0\%}$ fb	$7.16^{+3.1\%}_{-2.1\%}$ fb
no $gg \rightarrow \text{HZ}$, high- $p_{t,Z}$	$1.13^{+5.9\%}_{-5.3\%}$ fb	$1.21^{+0.1\%}_{-0.2\%}$ fb	$1.21^{+0.2\%}_{-0.3\%}$ fb	$1.13^{+1.5\%}_{-1.2\%}$ fb
with $gg \rightarrow \text{HZ}$, high- $p_{t,Z}$	–	$1.49^{+5.3\%}_{-4.1\%}$ fb	$1.48^{+5.3\%}_{-4.0\%}$ fb	$1.42^{+6.9\%}_{-5.1\%}$ fb

Table 1. Fiducial cross section of $pp \rightarrow \text{HZ} \rightarrow (b\bar{b})(e^+e^-)$ at 13 TeV with leptonic and b -jet cuts. The uncertainty band refers to the scale variation described in the text. Numerical errors for each prediction are beyond the quoted digits.

defined using the flavour- k_t algorithm [48] with $R = 0.4$. In the flavour- k_t algorithm we only consider b -quarks to be flavoured, and all other light quarks to be flavourless. Using b -tagging, such an algorithm can be implemented in experimental analyses. The fiducial cross sections in this phase-space volume at different levels of our simulations, are reported in Tab. 1. We also present results with an additional cut on the Z boson transverse momentum, $p_{t,Z} > 150$ GeV, which we refer to as high- $p_{t,Z}$ region.

We first discuss the results without $gg \rightarrow \text{HZ}$ contribution, over the full range of Z boson transverse momentum reported in the first line of the Tab. 1. The HZJ-MiNLO cross section is about 8% smaller than the full NNLO calculation from MCFM-8.0. The difference is properly accounted for by reweighting the event sample and the cross section of HZ-NNLOPS (LHEF) and MCFM-8.0 are equal to each other within the numerical accuracy (which is at the level of the last quoted digit). The scale uncertainty from the NLO result is reduced from about 7% to below 1% at the NNLO level. The inclusion of the $\mathcal{O}(\alpha_s^2)$ $gg \rightarrow \text{HZ}$ channel, reported in the second line of the table, results in further increase of the total cross section by about 10%. In this case, the scale uncertainty is dominated by the new contribution, which is described only at leading order, and increases the scale uncertainty to the level of 2-3%. This larger scale uncertainty is somehow welcome, as a scale uncertainty below the percent level is unlikely to reflect the true perturbative uncertainty. This uncertainty will be reduced by an NLO treatment of the $gg \rightarrow \text{HZ}$ contribution.²

We now discuss the impact of the parton shower on these cross sections. As is well known, in the presence of fiducial cuts that constrain the jet activity, as is in the case at hand, there can be a sizeable difference between a pure fixed-order computation and results after applying a parton shower. This is illustrated in the last two columns of the table. The parton shower allows for extra QCD radiation off coloured partons which can move the b -jets outside the fiducial phase-space volume, thereby reducing the recorded cross section. The impact of parton shower is similar in both instances, with and without the $gg \rightarrow \text{HZ}$ contribution, and amounts to about 10% reduction of the cross section in the fiducial region, while the impact is milder, 5 – 7%, in the high- $p_{t,Z}$ region.

If we now examine the results with an additional $p_{t,Z}$ cut, reported in the last two lines of the table, we observe a reduction of the cross section by a factor of about 5 and in general

²Note that the small difference in the $gg \rightarrow \text{HZ}$ contribution in MCFM-8.0 and HZ-NNLOPS (LHEF) is due to using LHAPDF or POWHEG routines to perform the running of the coupling from M_Z to the central scale choice $M_H + M_Z$.

behaviours similar to the ones described above. One point to note is that the impact of the $gg \rightarrow \text{HZ}$ contribution is larger in this phase space region, which implies also larger scale uncertainties.

To further illustrate the effect of the $gg \rightarrow \text{HZ}$ channel, we present in Fig. 7 the differential distributions of the invariant mass of the HZ system and transverse momentum of the b -jet pair system ($p_{t,b\bar{b}}$) associated to the reconstruction of the Higgs boson momentum. To define the HZ-invariant mass we use the Monte Carlo truth, while $p_{t,b\bar{b}}$ is obtained by clustering events with the flavour- k_t algorithm with $R = 0.4$ and by summing the transverse momenta of the two b -jets. If more than two b -flavoured jets are found, one selects the pair whose invariant mass is closest to the Higgs invariant mass.³ We show results from the HZNNLOPS simulation before and after the inclusion of the $gg \rightarrow \text{HZ}$ contribution (blue and red respectively) together with the fixed-order NNLO prediction including the $gg \rightarrow \text{HZ}$ contribution (green). For the invariant mass distribution, the large impact of the $gg \rightarrow \text{HZ}$ contribution above the top threshold is evident. Similarly, the transverse momentum distribution is mostly affected by the $gg \rightarrow \text{HZ}$ contribution in the region between 150 and 200 GeV. In both cases the impact of $gg \rightarrow \text{HZ}$ remains large up to high scales.

The invariant mass distribution (left panel of Fig. 7) features an almost uniform shift between the fixed-order predictions (green) and the ones including parton shower evolution (red). As discussed in the previous paragraph, parton shower leads to a decrease in the fiducial cross section mainly due to the b -jet cuts. However, the HZ invariant mass is not strictly correlated with the Higgs kinematics (and hence with the b -jets from its decay). As a consequence, we observe a moderate and constant difference between MCFM-8.0 and HZNNLOPS.

On the other hand, the effect of the parton shower on the transverse momentum of the reconstructed Higgs boson (right plot of Fig. 7) is quite different. In this case, one can see that the parton shower has a sizeable effect for $p_{t,b\bar{b}} \gtrsim 120$ GeV, and that it smears the distribution in a non-uniform way. At larger values of $p_{t,b\bar{b}} \gtrsim 300$ GeV, the effect of the partons shower becomes much more modest. A more detailed discussion is presented in App. D.

As a next step, we want to study the quality of the Higgs boson reconstruction. In Fig. 8, we present a comparison of the transverse momentum distribution of the true Higgs boson, obtained using the momentum passed from the event generator before it splits to b -quarks and before any radiation off the b -quarks (labelled as **MC-truth**), and the $b\bar{b}$ -jet system, reconstructed with a flavour- k_t algorithm as described above. We compare two sets of plots obtained with a jet radius of $R = 0.4$ (upper plots) or $R = 0.7$ (lower plots).⁴ The plots show a comparison of the fixed-order results (green curve)⁵, the HZNNLOPS after parton shower evolution (red) and the MC-truth prediction obtained with HZNNLOPS after parton shower (blue). The baseline in the ratio plot is taken to be the latter. In the left panels the $gg \rightarrow \text{HZ}$ contribution is not included, whereas its effect is included in right panels.

³We do not distinguish between b and \bar{b} jets.

⁴We note that the fiducial cuts are applied on jets of $R = 0.7$ in this case.

⁵Note that here only the b -quarks from the Higgs decay are considered flavoured.

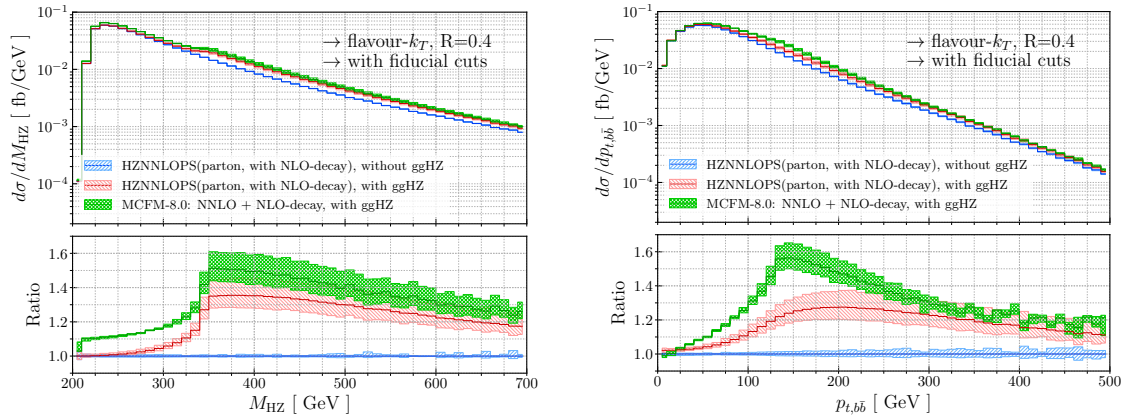


Figure 7. The differential distributions of the invariant mass of the HZ system (left panel) and the transverse momentum of the Higgs boson reconstructed from b -jets (right panel). The lower panel illustrate ratio of full results (NNLO as well as NNLOPS) to the NNLOPS results without $gg \rightarrow HZ$ contribution.

We start by examining the results without $gg \rightarrow HZ$ contribution (left hand panels). We note that both the fixed-order (green) and the HZNNLOPS after parton shower (red) differ from the MC-`truth` result (blue). At low transverse momenta, this difference becomes smaller when a larger jet-radius is considered (left bottom panel), which suggests that the dominant reason for the difference is out-of-jet radiation from the $b\bar{b}$ -final state. At larger transverse momenta the difference with respect to the MC-`truth` is instead smaller at smaller jet-radius (top left panel), which points to the fact that in this region the difference is mainly due to radiation from the initial state. We also notice that in the intermediate transverse momentum region the fixed-order and HZNNLOPS show sizeable differences for small jet radius, while these differences are more moderate when using a larger R . This can be easily understood from the fact that the observable with larger R is more inclusive and hence fixed-order and parton shower results are in better agreement.

We now move to discuss the plots including the $gg \rightarrow HZ$ effects. First, we note that the red and green bands in the top right panel of Fig. 8 are identical to the bands shown in the right panel of Fig. 7. As expected when the radius becomes bigger (bottom right panel) the fixed-order (green) and parton shower results (red) move closer to each other, again because the observables become more inclusive. We also note that the uncertainty bands are now larger compared to the results without $gg \rightarrow HZ$ contribution. This was already observed for the fiducial cross section and is due to the leading order description of the $gg \rightarrow HZ$ contribution.

We now show the distribution of the transverse momentum of the $b\bar{b}$ -jet system in the fiducial volume with and without the additional cut $p_{t,Z} > 150$ GeV. The relevant plots are shown in Fig. 9. First of all we note that the difference between treating the $H \rightarrow b\bar{b}$ decay at NLO with respect to LO is very small, which leads to the conclusion that a parton shower equipped with Matrix Element corrections to the $H \rightarrow b\bar{b}$ branching provides a very good estimation of the higher-order corrections. We also notice a Sudakov shoulder in the fixed-

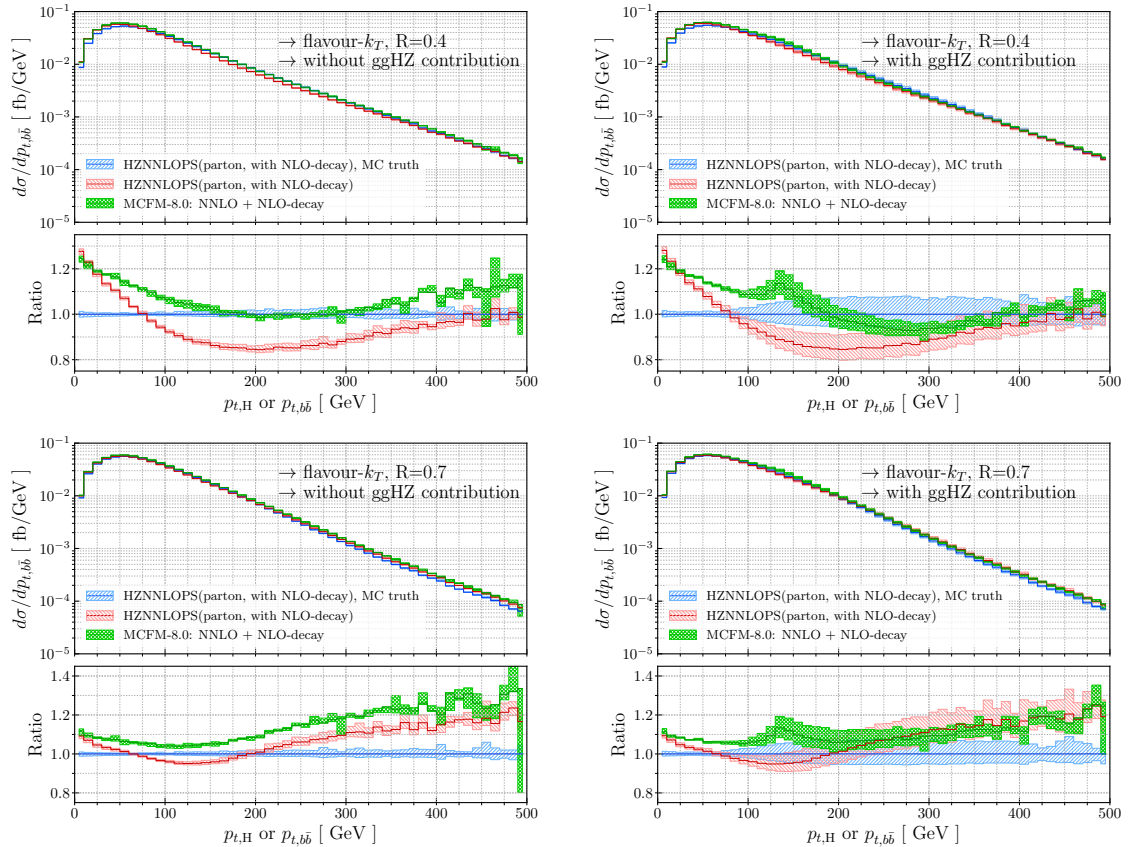


Figure 8. The differential distributions of the transverse momentum of the Higgs boson. **MC-truth** label refers to the actual Higgs boson momentum as passed from the event generator, other lines represent the reconstruction of the Higgs boson momentum using the two b -jets with invariant mass closest to M_H . The upper two plots show results for jets clustered with $R = 0.4$, the lower plots $R = 0.7$. Left plots do not include the $gg \rightarrow HZ$ contribution, while the right plots do.

order prediction in the right panel of Fig. 9 at $p_{t,b\bar{b}} = 150$ GeV. This feature has already been observed in Figs. (6) and (12) of ref. [9] and is due to the fact that the presence of the $p_{t,Z} > 150$ GeV cut makes the differential spectrum sensitive to soft gluon emission close to the cut. As expected, a parton shower captures parts of the resummation effects and therefore the shoulder is not present in the NNLOPS predictions.

One of the most important variables when reconstructing a resonance is the invariant mass of its decay products, therefore we will focus on it in the following, in the boosted high- $p_{t,Z}$ region. At LO in the decay the $M_{b\bar{b}}$ distribution is an extremely narrow Breit-Wigner function, and receives sizeable corrections away from the peak only at higher-orders. We start by examining how well `Pythia8` can describe the decay of the Higgs boson by comparing two calculations that include LO or NLO decay in the matrix element. When the matrix element is computed at LO only, `Pythia8` performs the shower using with hardness scale given in the Les Houches event file. This comparison is shown in Fig. 10 without (left plot) and with $gg \rightarrow HZ$ (right plot). We compare HZNNLOPS with LO treatment of

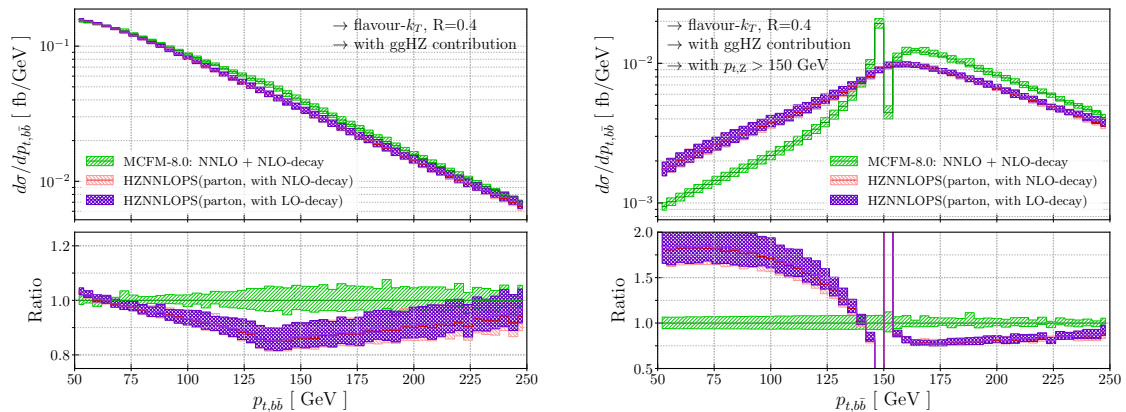


Figure 9. The differential distribution of the transverse momentum of the $b\bar{b}$ -jet system without (left) and with (right) the cut $p_{t,Z} > 150$ GeV. Results include the $gg \rightarrow HZ$ contribution.

the Higgs decay (purple), HZNNLOPS with NLO corrections to the $H \rightarrow b\bar{b}$ decay (red) and HZJ-MiNLO predictions, with NLO decay (green). We see that the two HZNNLOPS predictions are compatible with each other all the way down to relatively low $M_{b\bar{b}}$ masses. We note that the scale uncertainty is very small, of the order of 2-5%, when no $gg \rightarrow HZ$ contribution is included. This uncertainty increases when $gg \rightarrow HZ$ events are included, since these events sit at $M_{b\bar{b}} = M_H$ before showering. The small scale variation band is not indicative of the true uncertainty on this distribution and is related to the fact that HZJ-MiNLO results have been reweighted to NNLO results. In fact, the pure HZJ-MiNLO predictions, even without $gg \rightarrow HZ$, have a larger uncertainty. We also note that this uncertainty is also somehow underestimated as the band does not cover the HZNNLOPS results. This is related to the well known fact that, in a plain POWHEG simulation, the scale is varied at the level of the \bar{B} function, which is by definition inclusive over radiation, whereas the $M_{b\bar{b}}$ spectrum is sensitive to radiation.

In Fig. 11 we now compare fixed-order predictions (green) and our best prediction HZNNLOPS with NLO corrections to the $H \rightarrow b\bar{b}$ decay (red). In the plots of Fig. 11 we show predictions obtained with b -jets clustered with $R = 0.4$ (top panels) and $R = 0.7$ (bottom panels). We point out that in order to populate the region to the left of the peak ($M_{b\bar{b}} < M_H$) there must be a radiation off the b -quarks produced in the Higgs decay. On the contrary, the region on the right hand side of the peak ($M_{b\bar{b}} > M_H$) is filled only when additional radiation, off the partons from the production stage, is clustered with the Higgs decay products.

In Fig. 11 we notice a sizeable enhancement in the $M_{b\bar{b}}$ distribution to the left of the Higgs peak. This enhancement was already observed in refs. [9, 20] and is even more dramatic in this case. If we compare our left plots to the Figs. (4) and (11) of ref. [9] we observe a larger K-factor. However there are a number of differences. First, the results of ref. [9] are obtained with $R = 0.5$. Second, our MCFM-8.0 predictions are obtained using massive b -quarks, while the NNLO-approx calculation shown in ref. [9] is obtained with massless b -quarks. Furthermore, the two computations use different fiducial cuts and in [9]

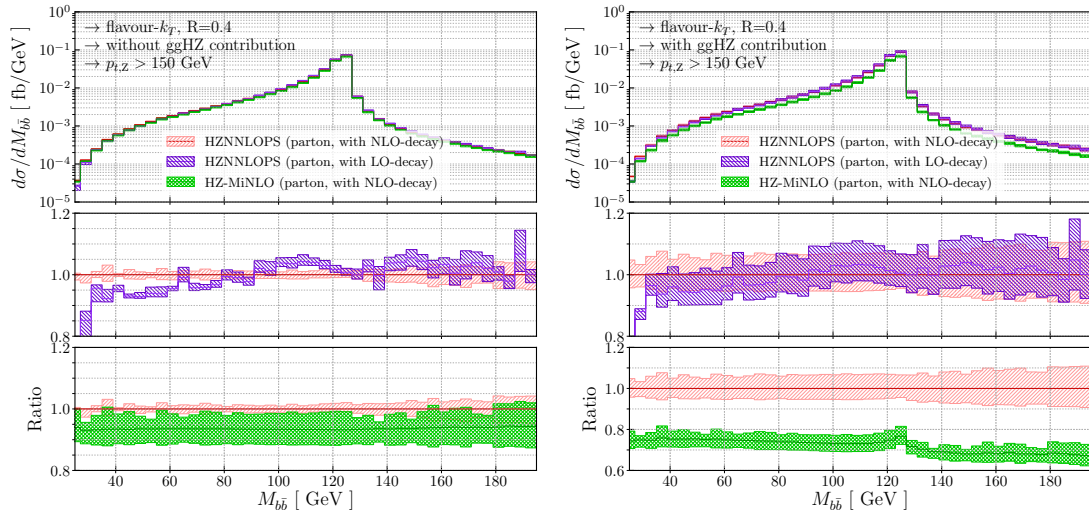


Figure 10. The differential distributions of the invariant mass of the $b\bar{b}$ -system used for reconstruction of the Higgs boson. Comparison of HZNNLOPS results with LO and NLO decay matrix elements, excluding $gg \rightarrow \text{HZ}$ channel (left panels) and with $gg \rightarrow \text{HZ}$ (right panels).

the process HW^- is considered, rather than HZ. Last, our plots show HZNNLOPS results rather than HZJ-MiNLO ones, and from Fig. 10 this amounts to a further increase of the ratio by 10% (25%) without (with) $gg \rightarrow \text{HZ}$. Similar considerations apply when comparing to Fig. (2) of ref. [20].

By looking at the plots on the right of Fig. 11, one can observe an even more pronounced enhancement of the HZNNLOPS over the MCFM-8.0 K-factor when the $gg \rightarrow \text{HZ}$ contribution is included. This is again due to the fact that the $gg \rightarrow \text{HZ}$ term in the fixed-order calculation is only in the $M_{b\bar{b}} = M_{\text{H}}$ bin, while this contribution is spread to other bins by the parton shower. A second observation is that when a large jet radius is considered (bottom row), more radiation is clustered in the b -jets. As a consequence, the distribution vanishes faster away from M_{H} . This effect is stronger when a parton shower is included and causes the K-factor to be smaller to the left of the peak and to even become close to one at very low mass.

Finally, in Fig. 12 we present the $M_{b\bar{b}}$ distribution obtained with HZNNLOPS at various stages after the Pythia8 parton showering, namely at parton-level and after hadronisation, with and without multi-parton interactions (MPI). We notice that hadronisation smears the distribution close to the peak. This is the reason for the dip at $M_{b\bar{b}} = M_{\text{H}}$ in the first inset. Away from the peak $M_{b\bar{b}} = M_{\text{H}}$, we observe that hadronisation effects become more important at low invariant masses, while, as expected, they become negligible at large $M_{b\bar{b}}$. Since color-connections tend to reduce spatial distances between partons during hadronisation, more radiation is clustered within the b -jets. This is the reason why the small $M_{b\bar{b}}$ regions are underpopulated with respect to predictions at parton level. This effect is similar with or without MPI. On the contrary, we can see a substantial change when considering MPI in the region $M_{b\bar{b}} > M_{\text{H}}$. Since MPI provide more radiation activity,

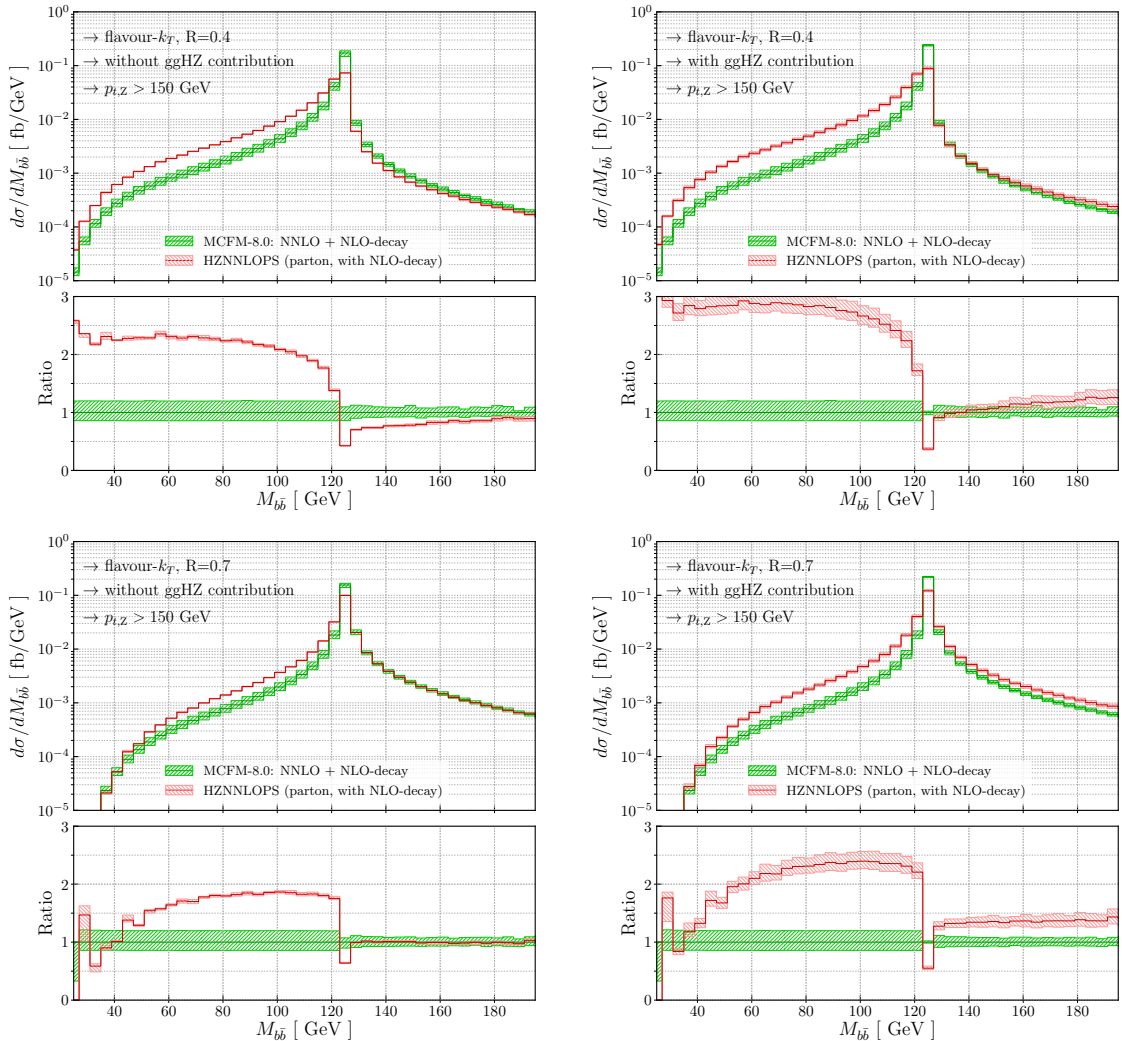


Figure 11. The differential distributions of the invariant mass of the $b\bar{b}$ -system used for reconstruction of the Higgs boson. We present the results obtained with jet clustering with $R = 0.4$ (top) and $R = 0.7$ (bottom) excluding $gg \rightarrow \text{HZ}$ channel (left panels) and with $gg \rightarrow \text{HZ}$ (right panels).

many additional hadrons can be clustered within the b -jets, thereby increasing the invariant mass of the $b\bar{b}$ -system and causing migration of events from the region $M_{b\bar{b}} \approx M_H$ to larger invariant masses.

6 Conclusions

In this paper we have implemented a consistent matching of NNLO accurate predictions for HZ production to parton shower, including the subsequent decay of the Z boson into pair of leptons and the NLO decay of the Higgs boson into pair of b -quarks. The HZNNLOPS generator we obtained allows for a fully-exclusive simulation of the HZ production in a hadronic collision maintaining the advantages of the NNLO fixed-order calculation and supplying it with resummation effects as provided by the matching to a parton shower.

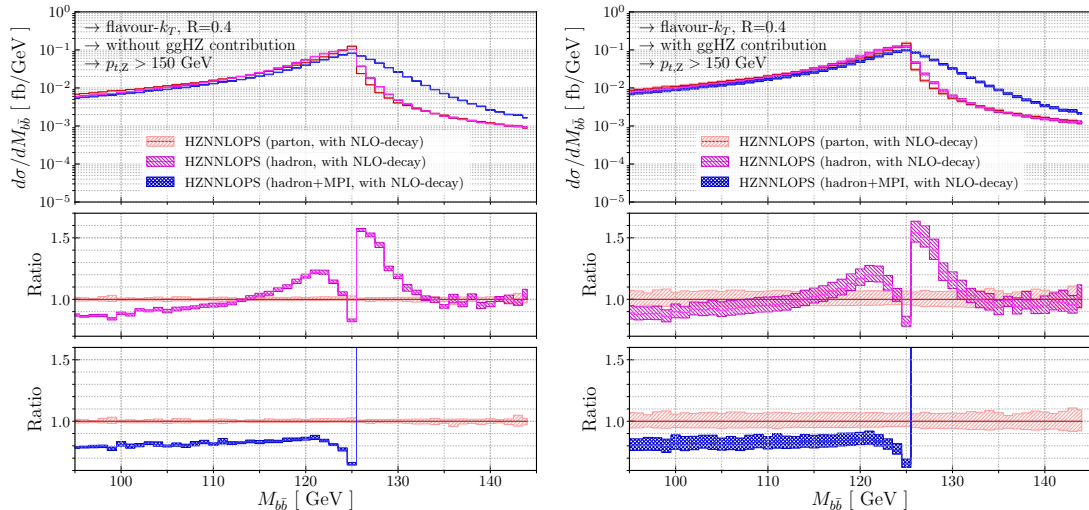


Figure 12. The differential distributions of the invariant mass of the $b\bar{b}$ -system used for reconstruction of the Higgs boson. Comparison of HZNNLOPS results with NLO decay matrix elements at parton-, hadron-level and with multi-parton interactions (MPI), excluding $gg \rightarrow HZ$ channel (left panels) and with $gg \rightarrow HZ$ (right panels).

In order to obtain this accuracy, we have extended the existing HZJ-MiNLO implementation to include the NLO corrections to the $H \rightarrow b\bar{b}$ decay. The NNLO+PS matching procedure requires a reweighting of the HZJ-MiNLO events that is fully-differential in the HZ Born kinematics. By using properties of the matrix elements at hand, we have parametrised the latter using variables that allow to express the differential cross section in terms of a finite set of functions, thereby simplifying considerably the multi-differential reweighting procedure. We have also included in the simulation the loop-induced $gg \rightarrow HZ$ channel that enters at $\mathcal{O}(\alpha_s^2)$, as it constitutes a sizeable part of the total cross section, and can give rise to substantial distortions of kinematic distributions.

In Sec. 5, we have considered a setup similar to the one used in searches for the Higgs decay into b -quarks. We find that scale uncertainties are substantially reduced when the NNLO corrections are included. Moreover we notice that the cross section in the fiducial region is reduced by about 5-10% during parton shower evolution as a consequence of requiring two b -jets satisfying the fiducial cuts. This correction brings the final result outside the NNLO uncertainty band. This highlights the limitation of using the scale uncertainty as an estimate of the true theoretical error associated to missing higher orders, in particular when more exclusive fiducial cuts are applied. A NNLO+PS simulation allows to capture some of these higher order effects, albeit with limited logarithmic accuracy.

As already noted in the literature, we also find that the $gg \rightarrow HZ$ channel has a significant impact, especially for the $M_{HZ} > 2m_t$ part of the spectrum. Moreover its presence has a very strong impact on the size of the scale uncertainty band. Since this contribution only enters at $\mathcal{O}(\alpha_s^2)$ level, in order to reduce this uncertainty one needs to include higher-order corrections to the discussed channel, which are currently unknown.

We also notice differences between distributions of the transverse momentum of the

Higgs boson, computed using Monte Carlo truth, and the transverse momentum of the $b\bar{b}$ -system identified and used for the reconstruction of the Higgs boson momentum. We point out that, especially when a large jet-radius is used, the amount of radiation clustered into b -jets leads to a harder p_T -spectrum than the one of the true Higgs boson.

Despite the consistency of the procedure we used in our simulation, we have obtained a large K-factor in the $M_{b\bar{b}} < M_H$ region of the distribution of the invariant mass of the $b\bar{b}$ -system. We also point out that the scale uncertainty of the NNLOPS prediction in this part of the spectrum is underestimated, due to known properties of the algorithm used by POWHEG to generate real radiation. These two issues will certainly require further studies. Including NNLO corrections to the $H \rightarrow b\bar{b}$ decay and matching them to parton showers would also be desirable, as well as trying to incorporate NLO electroweak effects as obtained in ref. [13]. We leave this to future work.

Acknowledgments

We would like to thank Gavin Salam for providing a private implementation of the flavour- k_t algorithm [48]. We also are grateful to Fabrizio Caola and Gionata Luisoni for providing some results of ref. [9] for cross-checks and to John Campbell, Giancarlo Ferrera, Keith Hamilton, and Paolo Nason for useful discussions. This work was supported in part by ERC Consolidator Grant HICCUP (No. 614577). The work of ER is supported by a Maria Skłodowska-Curie Individual Fellowship of the European Commission’s Horizon 2020 Programme under contract number 659147 PrecisionTools4LHC. WA and WB thank CERN for their hospitality while part of this work was done.

A Treatment of the $H \rightarrow b\bar{b}$ decay at NLO

The NLO corrections to the Higgs boson decay into two fermions $f\bar{f}$ have been known for a long time [14–17]. We have included them in the HZJ-MiNLO generator by extending the lists of the flavour structures considered by the process at hand to contain $b\bar{b}$ and $b\bar{b}g$ from the Higgs decay; creating the lists for the corresponding resonance structures; and by modifying the functions `setborn`, `setvirtual`, and `setreal` to supply amplitudes for the decay. The virtual corrections have been stripped of infra-red and ultra-violet singularities as described in section 2.4 of [49]. The relevant formulae read

$$\left| \mathcal{M}_{Hb\bar{b}}^{(0)}(p_H) \right|^2 = 2\sqrt{2}N_c G_F p_H^2 \beta^2 m_b^2(\mu_r), \quad (\text{A.1})$$

$$\begin{aligned}
2\Re\left(\mathcal{M}_{Hbb}^{(0)}(p_H)^* \mathcal{M}_{Hbb}^{(1)}(p_H)\right) &= \left|\mathcal{M}_{Hbb}^{(0)}(p_H)\right|^2 C_F\left(\frac{\alpha_s}{2\pi}\right) \\
&\times \left\{ -2 - 4\log(2) + \frac{1+\beta^2}{\beta} \left(\frac{2\pi^2}{3} + 2\text{Li}_2(\xi)\right) \right. \\
&\quad + \frac{1+\beta^2}{2\beta} \log(\xi) \left[\log(\xi) + 4\log(\beta)\right] \\
&\quad + \frac{1-\beta^2}{\beta} \left[-2\log(\xi)\right] + 2\left[\log(1-\beta) + \log(1+\beta)\right] \\
&\quad \left. - \left[\frac{1+\beta^2}{\beta} \log(\xi) + 2\right] \log\left(\frac{\mu_r^2}{p_H^2}\right) + \left[-3\log\left(\frac{m_b^2}{\mu_r^2}\right) + 4\right] \right\}, \quad (\text{A.2})
\end{aligned}$$

$$\begin{aligned}
\left|\mathcal{M}_{Hbbg}^{(0)}(p_H, q_1, q_2)\right|^2 &= \left|\mathcal{M}_{Hbb}^{(0)}(p_H)\right|^2 C_F\left(\frac{\alpha_s}{2\pi}\right) \cdot \frac{4\pi^2}{p_H^2 \beta^2} \left[8 + 4\frac{q_1 \cdot k}{q_2 \cdot k} + 4\frac{q_2 \cdot k}{q_1 \cdot k} \right. \\
&\quad + \beta^2 \left(\frac{p_H^2}{q_1 \cdot k} \frac{p_H^2}{q_2 \cdot k} - \frac{1}{2} \left(\frac{p_H^2}{q_1 \cdot k}\right)^2 - \frac{1}{2} \left(\frac{p_H^2}{q_2 \cdot k}\right)^2 - 4\frac{p_H^2}{q_1 \cdot k} - 4\frac{p_H^2}{q_2 \cdot k} \right) \\
&\quad \left. + \beta^4 \left(\frac{1}{2} \left(\frac{p_H^2}{q_1 \cdot k}\right)^2 + \frac{1}{2} \left(\frac{p_H^2}{q_2 \cdot k}\right)^2 + \frac{p_H^2}{q_1 \cdot k} \frac{p_H^2}{q_2 \cdot k} \right) \right], \quad (\text{A.3})
\end{aligned}$$

where p_H is the momentum of Higgs boson, q_1 and q_2 are the momenta of the b and \bar{b} quarks respectively, k is the momentum of the gluon in the real radiation matrix element,

$$x_b^2 = \frac{m_b^2}{p_H^2}, \quad \beta = \sqrt{1 - 4x_b^2}, \quad \text{and} \quad \xi = \frac{1 - \beta}{1 + \beta}. \quad (\text{A.4})$$

With $m_b(\mu_r)$ we denote the b -quark mass in the $\overline{\text{MS}}$ scheme, evaluated at the decay renormalisation scale μ_r . For the case at hand, we pick the Higgs boson mass as the central value for μ_r and its variation is correlated with the production renormalisation scale variation, *i.e.* we use the same scaling factor for μ_r and μ_R (where the latter is the renormalisation scale used for the production matrix elements, as introduced in Sec. 2.1). The last term in Eq. (A.2) denotes a change from on-shell scheme to $\overline{\text{MS}}$ scheme, namely using Eq. (63) of ref. [50] and retaining terms up to $\mathcal{O}(\alpha_s)$.

B Spectral decomposition of polar angle distributions

It is natural to use a spectral decomposition in terms of Fourier modes when dealing with an angular variable. The polar angle α that we use to parametrise the kinematics is defined on the interval $[0; \pi]$. The most generic parametrisation of the angular dependence can be written in terms of polynomials of $\cos \alpha$ and $\sin \alpha$ (note that quadratic and higher terms in $\sin \alpha$ can always be reduced to at most linear piece):

$$F(\alpha) = \sum_{a=0}^{\infty} \left(C_{1,a} (\cos \alpha)^a + C_{2,a} (\sin \alpha) (\cos \alpha)^a \right), \quad (\text{B.1})$$

which equivalently reads

$$\begin{aligned} F(x) &= \sum_{a=0}^{\infty} \left(C_{1,a} x^a + C_{2,a} \left(\sqrt{1-x^2} \right) x^a \right) \\ &= \sum_{i=0}^{\infty} \bar{C}_i f_i(x) \end{aligned} \quad (\text{B.2})$$

with

$$\begin{aligned} f_i(x) &= \left(\sqrt{1-x^2} \right)^{\text{mod}(i,2)} x^{\lfloor i/2 \rfloor}, \\ x &= \cos \alpha, \quad x \in [-1; +1]. \end{aligned} \quad (\text{B.3})$$

The above f_i functions are not orthonormal. Equipped with a scalar product between two functions

$$\langle F|G \rangle \equiv \int_{-1}^{+1} F(x) G(x) dx, \quad (\text{B.4})$$

we can transform the basis of functions $\{f_i\}$ into an orthonormal set $\{g_j\}$ by means of a Gram-Schmidt recurrence relation

$$\begin{aligned} k=0 : & \begin{cases} \tilde{g}_0 = f_0, \\ g_0 = \tilde{g}_0 / \langle \tilde{g}_0 | \tilde{g}_0 \rangle \end{cases} \\ k>0 : & \begin{cases} \tilde{g}_k = f_k - \sum_{j=0}^{k-1} \langle g_j | f_k \rangle \cdot g_j, \\ g_k = \tilde{g}_k / \langle \tilde{g}_k | \tilde{g}_k \rangle \end{cases} \end{aligned} \quad (\text{B.5})$$

and express a generic function F in terms of the $\{g_j\}$ basis

$$F(x) = \sum_{j=0}^N c_j g_j(x), \quad \text{with} \quad c_n = \langle g_n | F \rangle. \quad (\text{B.6})$$

For the case at hand, due to the arguments given in App. C, only terms up to $N = 10$ are needed.

C Hadronic tensor approach to matrix element

Hadronic collisions of protons are inherently linked with non-perturbative aspects of strong interactions through proton parton distribution functions (PDFs). Nevertheless we can use Lorentz symmetries and gauge invariance to predict the tensor structures that appear in matrix elements for associated Higgs production in pp collision. We distinguish two stages of the process: the production of the off-shell gauge boson in hadronic collision, that may be parametrised by the hadronic tensor, $H_{\mu\nu}$, and decay of the gauge boson into the Higgs boson and a pair of leptons, described by the decay tensor, $D_{\mu\nu}$. Since we are considering only QCD corrections and do not consider interference effects between production and decay products of the Higgs boson, the full squared matrix element can be written as

$$|\mathcal{M}(p_1, p_2, q, \ell_1, \ell_2)|^2 = \frac{H_{\mu\nu}(p_1, p_2, q) \cdot D^{\mu\nu}(q, \ell_1, \ell_2)}{(q^2 - M_Z^2)^2 + M_Z^2 \Gamma_Z^2}, \quad (\text{C.1})$$

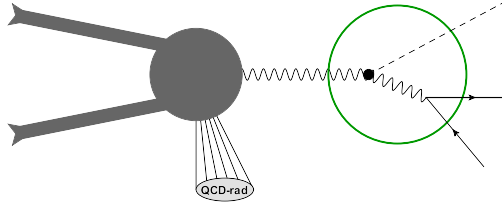


Figure 13. Amplitude for production of a weak gauge boson in proton-proton collision with subsequent branchings into Higgs boson and pair of leptons.

where p_1, p_2 are the momenta of the incoming protons, q is the momentum of the off-shell gauge boson before radiating off the Higgs boson, while ℓ_1 and ℓ_2 are the momenta of the two leptons that are produced. The momentum of the Higgs boson p_H may be obtained from conservation of momentum $p_H = q - \ell_1 - \ell_2$. We can parametrise the hadronic tensor as

$$H_{\sigma\sigma'} = (\varepsilon(q))_{\sigma}^{\mu} H_{\mu\nu}(p_1, p_2, q) (\varepsilon^*(q))_{\sigma'}^{\nu}, \quad (\text{C.2})$$

where the ε -four-vectors denote polarisation tensors of the gauge boson in the amplitude and its conjugate part, corresponding to polarisations σ and σ' respectively. The most general covariant form for the hadronic tensor [51, 52] reads

$$\begin{aligned} H_{\mu\nu}(p_1, p_2, q) = & H_1 \left(g_{\mu\nu} - \frac{q_{\mu}q_{\nu}}{q^2} \right) + H_2 \tilde{p}_{1\mu}\tilde{p}_{1\nu} + H_3 \tilde{p}_{2\mu}\tilde{p}_{2\nu} \\ & + H_4 (\tilde{p}_{1\mu}\tilde{p}_{2\nu} + \tilde{p}_{2\mu}\tilde{p}_{1\nu}) + H_5 (\tilde{p}_{1\mu}\tilde{p}_{2\nu} - \tilde{p}_{2\mu}\tilde{p}_{1\nu}) \\ & + H_6 \epsilon(\mu\nu p_1 q) + H_7 \epsilon(\mu\nu p_2 q) \\ & + H_8 (\tilde{p}_{1\mu} \epsilon(\nu p_1 p_2 q) + \{\mu \leftrightarrow \nu\}) + H_9 (\tilde{p}_{2\mu} \epsilon(\nu p_1 p_2 q) + \{\mu \leftrightarrow \nu\}), \end{aligned} \quad (\text{C.3})$$

where $\tilde{p}_{i\mu} = p_{i\mu} - (p_i q)/q^2 q_{\mu}$.

The decay tensor, $D_{\mu\nu}$, responsible for the part of the process that is represented inside a green circle in Fig. 13, can be parametrised as $D_{\sigma\sigma'} = (\varepsilon(q))_{\mu,\sigma} D^{\mu\nu}(q, \ell_1, \ell_2) (\varepsilon^*(q))_{\nu,\sigma'}$, where $D^{\mu\nu}(q, \ell_1, \ell_2)$ has the structure (for simplicity we omit overall coupling constant factors)

$$D^{\mu\nu} = \frac{g^{\mu\alpha} \left(-g_{\alpha\tilde{\alpha}} + \frac{k_{\alpha}k_{\tilde{\alpha}}}{M_Z^2} \right) L^{\tilde{\alpha}\tilde{\beta}} \left(-g_{\tilde{\beta}\tilde{\nu}} + \frac{k_{\tilde{\beta}}k_{\tilde{\nu}}}{M_Z^2} \right) g^{\beta\nu}}{(k^2 - M_Z^2)^2 + M_Z^2 \Gamma_Z^2}, \quad (\text{C.4})$$

where $k = \ell_1 + \ell_2$ is the momentum of the gauge-boson after radiating off Higgs boson and

$$L^{\tilde{\alpha}\tilde{\beta}} = \text{Tr} \left[\gamma^{\tilde{\alpha}} (V_{\ell} + A_{\ell}\gamma_5) \not{\ell}_1 \gamma^{\tilde{\beta}} (V_{\ell} + A_{\ell}\gamma_5) \not{\ell}_2 \right], \quad (\text{C.5})$$

where V_{ℓ} and A_{ℓ} are vector and axial components of the coupling of the vector boson to lepton. We can express the lepton momenta as $\ell_1 = \ell$ and $\ell_2 = k - \ell$. Plugging this into Eq. (C.5) and then further into Eq. (C.4), we find out that the momentum k of the Z boson after radiating off the Higgs boson appears in the final amplitude in Eq. (C.1) with at most power 5. This argument is analogous to the one used in ref. [32] to obtain the general form of the angular dependence of Drell-Yan decays.

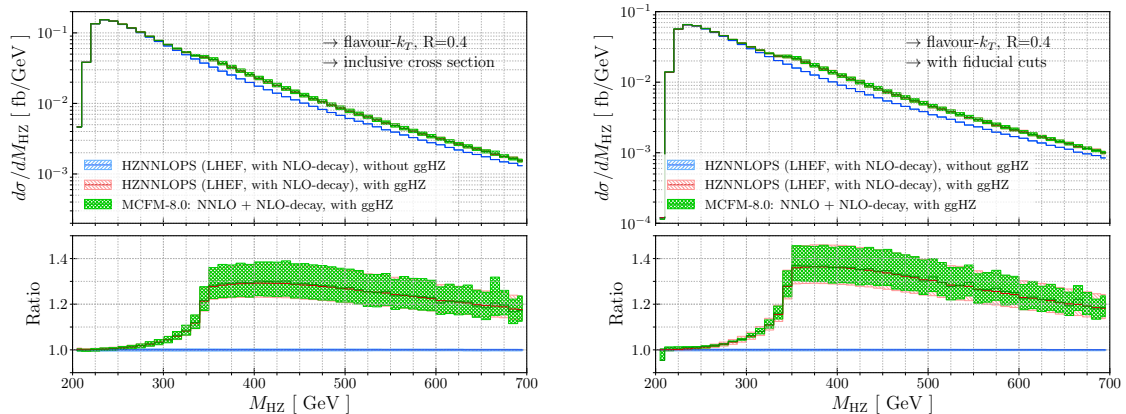


Figure 14. The differential distributions of the invariant mass of the HZ system at the LHEF level, without (left panel) and with fiducial cuts (right panel).

D Impact of the $gg \rightarrow HZ$ contributions

In this section we discuss the numerical impact of the loop-induced $gg \rightarrow HZ$ contribution, that we include as explained in Sec. 2.4. We will compare differential distributions obtained with the HZNNLOPS code and MCFM-8.0. The plots presented in this appendix show the result obtained at the level of Les Houches events before interfacing with parton shower. We will also comment on the differences with respect to the results after parton showering, shown in Sec. 5.

The effect of the $gg \rightarrow HZ$ contribution on the invariant mass of the HZ system is shown in Fig. 14, with the left and right panels showing the inclusive and fiducial distributions respectively. The distributions clearly show that, at LHEF level, the full HZNNLOPS result matches with MCFM-8.0, validating our procedure. One can also see that the $gg \rightarrow HZ$ contribution is significant when M_{HZ} is close to, or larger than, the $t\bar{t}$ threshold, and that the corrections remain large well above threshold. The application of fiducial cuts results in a further increase of the size of the corrections which is due to differences in acceptance rates for the two contributions (more than 60% $gg \rightarrow HZ$ events pass the cuts compared to $\sim 45\%$ HZ-NNLOPS(LHEF) events).

Similar considerations apply to the distribution of transverse momentum of the Higgs boson reconstructed from two b -jets whose invariant mass is closest to the Higgs mass. These distributions are shown in Fig. 15. One noticeable difference is that the effect of the $gg \rightarrow HZ$ dies out faster at large transverse momentum.

References

- [1] ATLAS collaboration, G. Aad et al., *Observation of a new particle in the search for the Standard Model Higgs boson with the ATLAS detector at the LHC*, *Phys. Lett.* **B716** (2012) 1–29, [[1207.7214](#)].
- [2] CMS collaboration, S. Chatrchyan et al., *Observation of a new boson at a mass of 125 GeV with the CMS experiment at the LHC*, *Phys. Lett.* **B716** (2012) 30–61, [[1207.7235](#)].

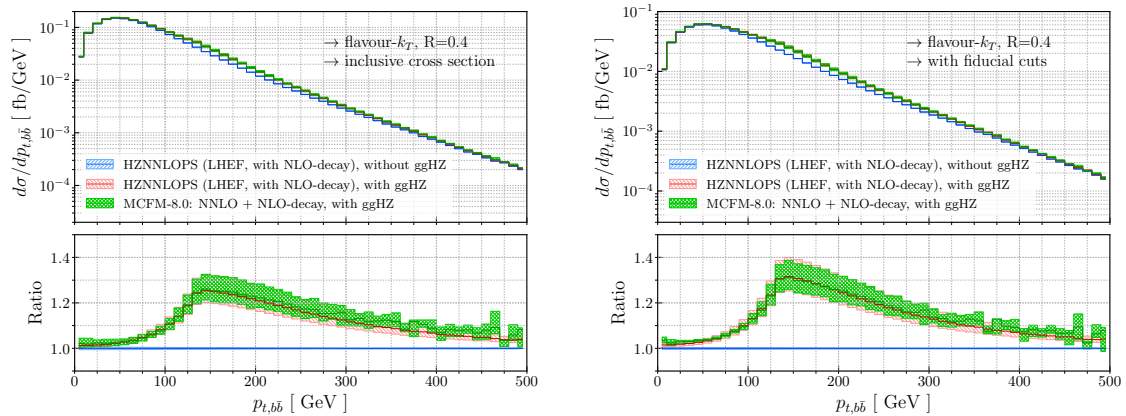


Figure 15. The differential distributions of the transverse momentum of the Higgs boson at the LHEF level, without (left panel) and with fiducial cuts (right panel).

- [3] ATLAS collaboration, M. Aaboud et al., *Evidence for the $H \rightarrow b\bar{b}$ decay with the ATLAS detector*, *JHEP* **12** (2017) 024, [[1708.03299](#)].
- [4] CMS collaboration, A. M. Sirunyan et al., *Evidence for the Higgs boson decay to a bottom quark–antiquark pair*, *Phys. Lett.* **B780** (2018) 501–532, [[1709.07497](#)].
- [5] G. Heinrich, *QCD calculations for the LHC: status and prospects*, in *5th Large Hadron Collider Physics Conference (LHCP 2017) Shanghai, China, May 15-20, 2017*, 2017. [1710.04998](#).
- [6] O. Brein, A. Djouadi and R. Harlander, *NNLO QCD corrections to the Higgs-strahlung processes at hadron colliders*, *Phys. Lett.* **B579** (2004) 149–156, [[hep-ph/0307206](#)].
- [7] G. Ferrera, M. Grazzini and F. Tramontano, *Associated ZH production at hadron colliders: the fully differential NNLO QCD calculation*, *Phys. Lett.* **B740** (2015) 51–55, [[1407.4747](#)].
- [8] J. M. Campbell, R. K. Ellis and C. Williams, *Associated production of a Higgs boson at NNLO*, *JHEP* **06** (2016) 179, [[1601.00658](#)].
- [9] F. Caola, G. Luisoni, K. Melnikov and R. Röntsch, *NNLO QCD corrections to associated WH production and $H \rightarrow b\bar{b}$ decay*, [1712.06954](#).
- [10] M. L. Ciccolini, S. Dittmaier and M. Kramer, *Electroweak radiative corrections to associated WH and ZH production at hadron colliders*, *Phys. Rev.* **D68** (2003) 073003, [[hep-ph/0306234](#)].
- [11] A. Denner, S. Dittmaier, S. Kallweit and A. Muck, *Electroweak corrections to Higgs-strahlung off W/Z bosons at the Tevatron and the LHC with HAWK*, *JHEP* **03** (2012) 075, [[1112.5142](#)].
- [12] A. Denner, S. Dittmaier, S. Kallweit and A. Mück, *HAWK 2.0: A Monte Carlo program for Higgs production in vector-boson fusion and Higgs strahlung at hadron colliders*, *Comput. Phys. Commun.* **195** (2015) 161–171, [[1412.5390](#)].
- [13] F. Granata, J. M. Lindert, C. Oleari and S. Pozzorini, *NLO QCD+EW predictions for HV and HV +jet production including parton-shower effects*, *JHEP* **09** (2017) 012, [[1706.03522](#)].

- [14] E. Braaten and J. P. Leveille, *Higgs Boson Decay and the Running Mass*, *Phys. Rev.* **D22** (1980) 715.
- [15] M. Drees and K.-i. Hikasa, *NOTE ON QCD CORRECTIONS TO HADRONIC HIGGS DECAY*, *Phys. Lett.* **B240** (1990) 455.
- [16] N. Sakai, *Perturbative QCD Corrections to the Hadronic Decay Width of the Higgs Boson*, *Phys. Rev.* **D22** (1980) 2220.
- [17] P. Janot, *First Order QED and QCD Radiative Corrections to Higgs Decay Into Massive Fermions*, *Phys. Lett.* **B223** (1989) 110–118.
- [18] C. Anastasiou, F. Herzog and A. Lazopoulos, *The fully differential decay rate of a Higgs boson to bottom-quarks at NNLO in QCD*, *JHEP* **03** (2012) 035, [[1110.2368](#)].
- [19] V. Del Duca, C. Duhr, G. Somogyi, F. Tramontano and Z. Trócsányi, *Higgs boson decay into b-quarks at NNLO accuracy*, *JHEP* **04** (2015) 036, [[1501.07226](#)].
- [20] G. Ferrera, G. Somogyi and F. Tramontano, *Associated production of a Higgs boson decaying into bottom quarks at the LHC in full NNLO QCD*, [1705.10304](#).
- [21] S. Höche, Y. Li and S. Prestel, *Drell-Yan lepton pair production at NNLO QCD with parton showers*, *Phys. Rev.* **D91** (2015) 074015, [[1405.3607](#)].
- [22] S. Höche, Y. Li and S. Prestel, *Higgs-boson production through gluon fusion at NNLO QCD with parton showers*, *Phys. Rev.* **D90** (2014) 054011, [[1407.3773](#)].
- [23] S. Alioli, C. W. Bauer, C. Berggren, F. J. Tackmann, J. R. Walsh and S. Zuberi, *Matching Fully Differential NNLO Calculations and Parton Showers*, *JHEP* **06** (2014) 089, [[1311.0286](#)].
- [24] K. Hamilton, P. Nason and G. Zanderighi, *MINLO: Multi-Scale Improved NLO*, *JHEP* **10** (2012) 155, [[1206.3572](#)].
- [25] K. Hamilton, P. Nason, C. Oleari and G. Zanderighi, *Merging H/W/Z + 0 and 1 jet at NLO with no merging scale: a path to parton shower + NNLO matching*, *JHEP* **05** (2013) 082, [[1212.4504](#)].
- [26] K. Hamilton, P. Nason, E. Re and G. Zanderighi, *NNLOPS simulation of Higgs boson production*, *JHEP* **10** (2013) 222, [[1309.0017](#)].
- [27] K. Hamilton, P. Nason and G. Zanderighi, *Finite quark-mass effects in the NNLOPS POWHEG+MiNLO Higgs generator*, *JHEP* **05** (2015) 140, [[1501.04637](#)].
- [28] A. Karlberg, E. Re and G. Zanderighi, *NNLOPS accurate Drell-Yan production*, *JHEP* **09** (2014) 134, [[1407.2940](#)].
- [29] W. Astill, W. Bizon, E. Re and G. Zanderighi, *NNLOPS accurate associated HW production*, *JHEP* **06** (2016) 154, [[1603.01620](#)].
- [30] T. Ježo and P. Nason, *On the Treatment of Resonances in Next-to-Leading Order Calculations Matched to a Parton Shower*, *JHEP* **12** (2015) 065, [[1509.09071](#)].
- [31] S. Frixione, P. Nason and C. Oleari, *Matching NLO QCD computations with Parton Shower simulations: the POWHEG method*, *JHEP* **11** (2007) 070, [[0709.2092](#)].
- [32] J. C. Collins and D. E. Soper, *Angular Distribution of Dileptons in High-Energy Hadron Collisions*, *Phys. Rev.* **D16** (1977) 2219.

- [33] B. Hespel, F. Maltoni and E. Vryonidou, *Higgs and Z boson associated production via gluon fusion in the SM and the 2HDM*, *JHEP* **06** (2015) 065, [[1503.01656](#)].
- [34] D. Goncalves, F. Krauss, S. Kuttimalai and P. Maierhöfer, *Higgs-Strahlung: Merging the NLO Drell-Yan and Loop-Induced 0+1 jet Multiplicities*, *Phys. Rev.* **D92** (2015) 073006, [[1509.01597](#)].
- [35] L. Altenkamp, S. Dittmaier, R. V. Harlander, H. Rzehak and T. J. E. Zirke, *Gluon-induced Higgs-strahlung at next-to-leading order QCD*, *JHEP* **02** (2013) 078, [[1211.5015](#)].
- [36] R. V. Harlander, A. Kulesza, V. Theeuwes and T. Zirke, *Soft gluon resummation for gluon-induced Higgs Strahlung*, *JHEP* **11** (2014) 082, [[1410.0217](#)].
- [37] C. Englert, M. McCullough and M. Spannowsky, *Gluon-initiated associated production boosts Higgs physics*, *Phys. Rev.* **D89** (2014) 013013, [[1310.4828](#)].
- [38] R. V. Harlander, S. Liebler and T. Zirke, *Higgs Strahlung at the Large Hadron Collider in the 2-Higgs-Doublet Model*, *JHEP* **02** (2014) 023, [[1307.8122](#)].
- [39] R. V. Harlander, J. Klappert, C. Pandini and A. Papaefstathiou, *Exploiting the WH/ZH symmetry in the search for New Physics*, [1804.02299](#).
- [40] G. Luisoni, P. Nason, C. Oleari and F. Tramontano, *$HW^\pm/HZ + 0$ and 1 jet at NLO with the POWHEG BOX interfaced to GoSam and their merging within MiNLO*, *JHEP* **10** (2013) 083, [[1306.2542](#)].
- [41] NNPDF collaboration, R. D. Ball et al., *Parton distributions for the LHC Run II*, *JHEP* **04** (2015) 040, [[1410.8849](#)].
- [42] L. A. Harland-Lang, A. D. Martin, P. Motylinski and R. S. Thorne, *Parton distributions in the LHC era: MMHT 2014 PDFs*, *Eur. Phys. J.* **C75** (2015) 204, [[1412.3989](#)].
- [43] S. Dulat, T.-J. Hou, J. Gao, M. Guzzi, J. Huston, P. Nadolsky et al., *New parton distribution functions from a global analysis of quantum chromodynamics*, *Phys. Rev.* **D93** (2016) 033006, [[1506.07443](#)].
- [44] S. Carrazza, J. I. Latorre, J. Rojo and G. Watt, *A compression algorithm for the combination of PDF sets*, *Eur. Phys. J.* **C75** (2015) 474, [[1504.06469](#)].
- [45] K. G. Chetyrkin, J. H. Kuhn and M. Steinhauser, *RunDec: A Mathematica package for running and decoupling of the strong coupling and quark masses*, *Comput. Phys. Commun.* **133** (2000) 43–65, [[hep-ph/0004189](#)].
- [46] T. Sjöstrand, S. Ask, J. R. Christiansen, R. Corke, N. Desai, P. Ilten et al., *An Introduction to PYTHIA 8.2*, *Comput. Phys. Commun.* **191** (2015) 159–177, [[1410.3012](#)].
- [47] J. M. Campbell, R. K. Ellis, P. Nason and E. Re, *Top-Pair Production and Decay at NLO Matched with Parton Showers*, *JHEP* **04** (2015) 114, [[1412.1828](#)].
- [48] A. Banfi, G. P. Salam and G. Zanderighi, *Infrared safe definition of jet flavor*, *Eur. Phys. J.* **C47** (2006) 113–124, [[hep-ph/0601139](#)].
- [49] S. Alioli, P. Nason, C. Oleari and E. Re, *A general framework for implementing NLO calculations in shower Monte Carlo programs: the POWHEG BOX*, *JHEP* **06** (2010) 043, [[1002.2581](#)].
- [50] J. M. Campbell, R. K. Ellis, F. Maltoni and S. Willenbrock, *Higgs-Boson production in association with a single bottom quark*, *Phys. Rev.* **D67** (2003) 095002, [[hep-ph/0204093](#)].

- [51] J. G. Korner and E. Mirkes, *Polarization density matrix of high $q(T)$ gauge bosons in high-energy proton - anti-proton collisions*, *Nucl. Phys. Proc. Suppl.* **23B** (1991) 9–13.
- [52] C. S. Lam and W.-K. Tung, *A Systematic Approach to Inclusive Lepton Pair Production in Hadronic Collisions*, *Phys. Rev.* **D18** (1978) 2447.